Title
Building New Tools to Measure Noise in Organelle Size Control

Permalink
https://escholarship.org/uc/item/2sb6t097

Author
Bauer, David Paul

Publication Date
2020

Peer reviewed|Thesis/dissertation

Building New Tools to Measure Noise in Organelle Size Control

by
David Bauer

DISSERTATION
Submitted in partial satisfaction of the requirements for degree of
DOCTOR OF PHILOSOPHY

in

Biophysics

in the

GRADUATE DIVISION
of the
UNIVERSITY OF CALIFORNIA, SAN FRANCISCO

Approved:

DocuSigned by:

Wallace Marshall _____
68DD18512B3C4D9...

Wallace Marshall
_____
Chair

DocuSigned by:

Sy Redding _____
DocuSigned by:441...

Sy Redding
_____

Sophie Dumont _____
8305715E0D454DC...

Sophie Dumont
_____

_____

_____
Committee Members

Building New Tools to Measure Noise in Organelle Size Control

Acknowledgments

First, I would like to thank Wallace for his guidance, support, and for creating a wonderful lab to work in, where you are so supported in all your endeavors. I am also very appreciative of Wallace's philosophy of science, particularly his vision of biology as an engineering discipline. I did not do a traditional biology PhD, and some PI's would not have fought as hard as Wallace did to enable my projects and goals.

It was such a pleasure to work with the other members of the Marshall Lab. Not only is everyone a brilliant scientist, but they are also genuinely great people to be around, both socially and professionally. I would particularly like to call out Athena on her commitment to making the lab a better place to work. Especially in organizing birthday/quals celebrations (with cake!), I think she put in more than a reasonable amount of time and effort for a grad student, and the lab benefited greatly from it.

I am also very grateful to Andy for the extraordinary amount of time he dedicated to mentoring me at Calico, and for working through so much bureaucracy to secure a joint position. I do not believe I could received the the same volume of one-on-one mentoring from a physics-based perspective at UCSF.

I would like to thank my parents, who have given me nothing but support throughout my entire academic career, never pressuring me to be anything but my best.

Finally, I could not have completed my PhD without the the support, wisdom, and companionship of Chelsea. I am so lucky to have such an amazing person with me for the

rest of my life.

Contributions

Parts of Chapter 2 appear in Wemmer, K. and Marshall, W. M. Architecture and Assembly of Chlamydomonas Flagella. 2011. University of California - San Francisco, PhD dissertation. https://escholarship.org/uc/item/41v540tt

Abstract

Building New Tools to Measure Noise in Organelle Size Control

by

David Bauer

Organelle size control is an interesting problem in Biology. Organelles are often difficult to label or shaped in a way that is difficult to quantify. Chlamydomonas reinhardtii is a single celled alga with two equal length cilia. These cilia represent an ideal case study for organelle size control. Their size is easily quantifiable, as they are essentially one dimensional, only changing in length. The cilia are shed under acid shock, and completely regenerate within two hours. Measurement of length as a function of time during regeneration provides a quantitative insight into the regeneration process, and represents a crucial measurement required to fit predictions of length control models. But obtaining such measurements has proven extremely difficult because Chlamydomonas cells swim rapidly through the media. As a result, regeneration timecourse data usually is obtained at a population level using fixed samples. To enable high-throughput measurements of Chlamydomonas cilia length in living cells, we built a microfluidic device capable of trapping Chlamydomonas and solution

exchange. Using this device, we found that instrinsic and extrinsic noise are present in the length control system. We were able to characterize the noise and assess its impact on biological function.

Contents

List of Figures

List of Tables

Chapter 1

Introduction

1.1   Organelle Size Control

There is often a dichotomy in science fiction: man vs machine. Often at odds with each other due to their "conflicting nature", one declares the other incompatible with their own and calls for the destruction of the other. Over the course of my PhD, I now fail to see a difference between the two. What is a cell, if not the most complex machine known to exist? Unfortunately, due to the meandering path evolution must follow to find the "fittest", cells do not resemble any machine humans have ever made. Compared to most machines we use today, they are slow, imprecise, and noisy. Yet, they are just as well suited to their tasks.

Every machine, whether biological or mechanical, requires proper manufacture of its components to function. This includes manufacturing components to the right size and shape. For example, in manufacturing a USB port, a connector outside the specified size

tolerance can result in a connector too small to receive a plug, or too large to maintain the necessary electrical contacts. Cells must also manufacture their components (such as organelles) within tolerance for proper function.

How cells control the size of their organelles is a long standing question in biology. Earlier than 100 years ago, scientists have noted patterns, such as the kern-plasma relation [42], in the size of subcellular structures. There have been studies that have found remarkable examples of size control. In bacteriophage lambda [22], a deletion in a particular gene produces a shortening in tail length equal to the size of the deletion. Even a single cell is an incredibly complex structure composed of many subcellular components. Further, cells themselves are highly dynamic; they must divvy themselves up to reproduce, ensuring that all daughter cells have the necessary components in the right amount. Some cells must drastically change shape in response to their environment. Cell morphology is an important problem to study that affects basic biological function.

Models of Organelle Size Control

The ultimate goal of studying organelle size control would to be able to create a mathematical model describing the shape, size, and number of any organelle, and be able to manipulate at will all of these properties. Perhaps due to the difficulty of describing the complicated, dynamic structures of the cell (golgi, endoplasmic reticulum, mitochondria), there have been few mathematical models. There have been many qualitative, and some quantitative de-

scriptions of organelle size control [32][36][9][30]. It is a strong possibility, given that each organelle was incorporated or evolved at different times in evolutionary history, that no such general model of organelle size control exists. A similar mechanism could be ultimately responsible for different organelles, but given the difference in function, it would not be surprising to find that each organelle has its own size control circuit. Some have proposed that size control is governed by a limited precursor [32]. In this model, the only lever the cell has for size control is production or reduction of precursor, and it serves as a "null" model. Recent work has shown that the limiting precursor model does not provide size control when there are multiple organelles, as is the case with *Chlamydomonas* flagella [41].

1.2   Chlamydomonas as a Model Organism

Chlamydomonas reinhardtii is a single celled alga with two equal length flagella. The cell body and the flagella are each about 10μm in length. *Chlamydomonas* has long been a model organism due its ease of culture and tractable genetics. There are also a variety of mutants with many different phentotypes of flagellar length, number, and regeneration kinetics, many with functional length control [8].

Chlamydomonas as a model for organelle size control

The *Chlamydomonas* flagella is an ideal organelle for organelle size control studies. Unlike other organelles, such as mitochondria or the endoplasmic reticulum, which have complicated
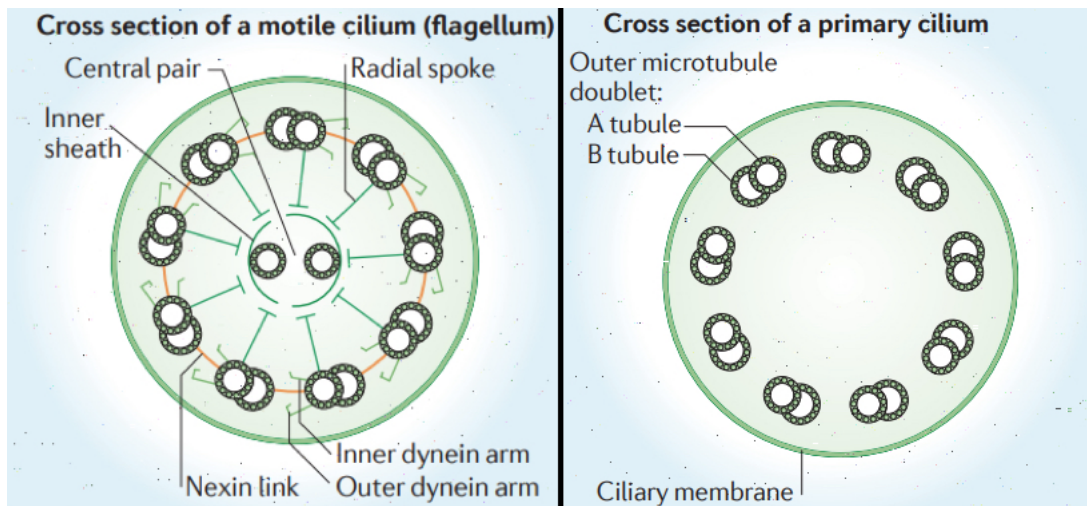
Figure 1.1: Cross section of a motile cilium (such as *Chlamydomonas* flagellum) vs. a non-motile primary cilium. Adapted from Ishikawa *et al.* 2011

geometry, the geometry of the *Chlamydomonas* flagella is simple. Changes in shape are unambiguous, as it can change in only one dimension. Furthermore, the shape of the flagella can be unambiguously specified by a single number: it's length. Despite it's simple structure, it shares a high degree of structural similarity to mammalian cilia, suggesting that a similar mechanism might be responsible for length control in both systems. As seen in Fig 1.1, the flagellar axoneme consists of 9 pairs of microtubule doublets surrounding a central pair of singlet microtubules.

1.3 Flagellar Length Control

Chlamydomonas has two 10μm length flagella, and they exhibit remarkable length control. Flagellar regeneration can be induced via pH-shocking, where the cell sheds it flagella and
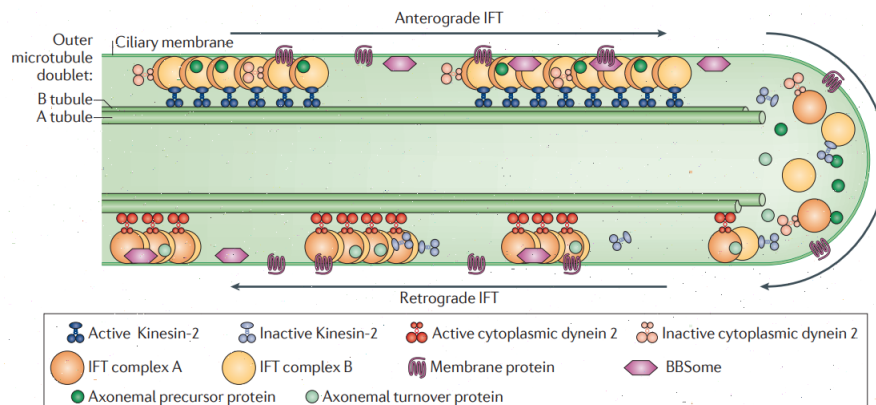
Figure 1.2: The known molecular players involved in intraflagellar transport (IFT). Adapted from Ishikawa *et al.* 2011

regrows them in about an hour. Throughout regrowth, the flagella are approximately equal, until they achieve approximately the same pre-shock length. Furthermore, if you mechanically sever just one of the cell's flagella, the longer flagella will shrink as the severed one regenerates until they are approximately equal length, after which they grow out together (referred to as the long zero experiment) [37]. *Chlamydomonas* clearly demonstrates that it possesses some method of length regulation, both in equilibrium length, and in terms of equilibrating the difference in length between the two flagella.

Biology of Flagellar Length Control

Although the exact mechanism of flagellar length control is still unkonwn, we still know many of the molecular players. Multiprotein complexes called Intra-Flagellar Transport (IFT) proteins contain binding sites for flagellar precursors, such as tubulin and flagellar membrane proteins. Multiple IFT form linear chains like a cargo train, are injected into the

proximal end of the cell, and carried from the proximal end of the axoneme to the distal end via Kinesin-2. At the distal end of the flagella, some of its cargo is incorporated into the flagella. Kinesin is deactivated, and cytoplasmic Dynein 2 carries the cargo back to the proximal end of the axoneme [19]. The flagella is thought to be under constant disassembly, at a rate that is constant and independent of length.

Biological Relevance of Flagellar Length Control

The similarity of structure of the flagellar axoneme in *Chlamydomonas* to the mammalian cilia suggests that similar mechanisms could be responsible for length control in both organisms. Many human diseases and disorders are associated with abnormal length flagella, such as retinitis pigmentosa [31] and Meckel-Gruber syndrome [5], and proper ciliary length and function are important in creating sidedness during development. Many mutations that affect flagellar length in *Chlamydomonas* are implicated in mammalian ciliopathies. For example, in the CEP290 mutant, *Chlamydomonas* flagella are short [11]. Cep290p is a protein that localizes to the transition zone near the basal body and flagellar membrane. Humans with mutations in CEP290 can have ciliopathies affecting every organ or tissue with cilia and symptoms that range from blindness to perinatal death, but CEP290 is just one of a family of genes that produce the same symptoms [15][17]. It is plausible that rescue of abnormal length flagella in *Chlamydomonas* could have translational value in mammalian ciliopathies.

1.4 Models of Flagellar Length Control

How this phenomenon of precise length control is achieved by the cell is still largely a mystery, but not for lack of ideas. There have been many attempts to model this behavior, although many have since proven unsuccessful. Models must be consistent with the experimental data observed to date, key aspects of which are 1/L length dependence of IFT [4] and thus active regulation of injection.

Limited Pool or Null Model

In static models where injection of IFT is not actively regulated in proportion to some kind of length signal, the size of the flagella is set by the availability of precursor. The cell can regulate the length of its flagella by upregulating or downregulating precursor. Because of the shared pool of precursor between the two flagella, with no mechanism regulating the length of each flagella, this model is not likely able to be responsible as shown in [41].

Swim Speed Model

The swim speed model [25] proposes that the flagellar membrane experiences stretching forces proportional to the flagellar beat frequency, and that this perturbation to the membrane allows for the passage of ions from the surrounding media into the flagella. In the swim speed model, these ions produce an inhibitory affect on IFT injection as they pass into the cell body. The swim speed model is not supported by experimental evidence [25]. Paralyzed

flagella mutants are often shorter, rather than longer as predicted. Further, increasing the viscosity of the media should increase the length of the flagella by increasing the strain on the flagellar membrane, but no such lengthening has been observed.

Time of Flight Model

In the time of flight model, some component used in flagellar assembly (for example, IFT) is modified to an excited state with a decay time comparable to the length of time it takes IFT to traverse to the tip of the flagella and back again. Longer flagella would have a higher proportion of components in the ground state relative to shorter flagella, producing a signal that could regulate flagellar assembly. Upon examination of this model [20], using mutants in retrograde transport that increase the overall traversal time of IFT particles within the flagellum, the authors found that injection of IFT is not controlled via a time of flight mechanism. Contrary to the model, IFT injection actually *increased* when retrograde IFT train speed was reduced. Given that the increased injection observed did not lead to an increase in flagellar length, it is possible that cargo-loading of IFT is regulated by a time of flight mechanism.

Ion Current Model

In the ion current model, ion channels embedded in the flagellar membrane provide a flux of ions that exit the flagellum at the ciliary pore. This current of ions leaving the flagellum

could have an inhibitory affect on flagellar assembly [18]. The ion current model is able to provide a length dependent signal because the total number of ion channels is dependent upon flagellar length. While other models depend on the linearity of the flagellum, the ion current model is generalizable to any membrane-bound organelle.

Diffusion Model

In the diffusion model as described by [13], the length control producing signal is the concentration gradient of kinesin along the flagellum produced by the diffusion of deactivated kinesin from the distal end back to the base. This model has been examined mathematically in [16], and has shown diffusion to be sufficient to serve as a biological ruler in the context of flagellar length control.

1.5 Using Noise in Biological Systems

As summarized above, there are many promising models of length control that are consistent with the data, which consist entirely of average flagellar lengths. The key goal of my dissertation has been to examine flagellar length control with a different type of data — length fluctuations. Using noise to get additional scientific insight is a technique that has been employed by other fields. In astronomy, type Ia supernovae, which are thought to inherently have very similar luminosities, deviate from their standardized luminosity [33][39]. Can these asymmetries tell us anything about Ia progenitors? Amir *et al.* ask similar questions about

the use of noise in biological systems, as well as considerations in mathematical modeling [21].

Given that progress has been made in mathematical descriptions of how size control circuits could work, the models can begin to make quantitative predictions not only about mean size, but also about when the size control circuit is "wrong/off target". Because the scale of cells is constantly flirting with the diffraction limit, it is fortunate for biology that cells are so noisy. Chlamydomonas flagella, with a mean length of approximately 10 μm, experience fluctuations about their mean length by approximately 10% (discussed further Chapter 2), which is well above the diffraction limit. Note that the noise we are discussing is real noise present in the system we are measuring with a biological or physical basis, and not noise injected into our measurement via electronics or human error.

An example of how this could contribute to flagellar length control in Chlamydomonas is described by [23]. In this work, Fai *et al.* create mathematical models for length control with varying assumptions based on possible biological mechanisms. After arriving at an equation that describes the steady state flagellar length, they linearize the equation to get an equation that describes how that model would respond to small perturbations around the steady-state length. The authors are able to make predictions about the timescale on which these fluctuations would be resolved, which are different depending on the assumptions of the model. However, the work in Fai *et al.* is entirely theoretical and will require actual measurement of length fluctuations in the flagellar length control system.

Intrinsic and Extrinsic Noise

Noise can arise from different processes in the cell, and are sometimes physically distinguishable from one another. Two such categories of noise in biological systems were coined by Elowitz *et al* [38]. To investigate the extent and effects of stochasticity in gene expression, they look at expression of two different fluorescent proteins driven by identical promoters, and find the noise "intrinsic to the expression of this gene" where the noise arises mostly from small number statistics from a small number of components (like the processivity of a single polymerase), and noise "extrinsic to the expression of this gene" to mean the average value (not small number statistics) of everything else that affects gene expression over the entire cell, such as larger cells having more ribosomes. There may be additional sources of extrinsic noise, discussed in Chapter 2.

We can apply the same concepts to describe flagellar length control, where noise processes that happen inside the flagella are instrinsic noise, and processes that happen outside the flagellum are extrinsic noise. Extrinsic noise would thus include noise present in the cell body, as well as noise present in the extracellular environment. Operationally, intrinsic noise manifests as changes in length between the two flagellum, and extrinsic noise as changes in mean length of both flagella.

1.6 Cell Size Control

In addition to subcellular size control, it is also generally unknown how a cell regulates its overall size. There are models for various ways that cells can monitor their own size, and decide when to divide. Consider a cell population where a single cell's time between division is described by:

$$t_d = \langle t_d \rangle - \alpha \log \frac{\langle V_b \rangle}{V_b} \tag{1.1}$$

where t_d is the time between division, $\langle t_d \rangle$ is the average time between division, V_b is the volume of the cell at birth, $\langle V_b \rangle$ is the average volume of the cell at birth, and α is a parameter encompassing the size-control mechanism. There are three potential models for how cells achieve size control. First, in the sizer model, a cell monitors its own size, and does not proceed through cell division until a threshold of absolute size has been reached. This corresponds to $\alpha = 1$. In an adder model, cells add a fixed size increment. This corresponds to $\alpha = 0.5$. In a timer model, cells grow for a fixed time duration and then divide, regardless of cell size, so $t_d = \langle t_d \rangle$ and $\alpha = 0$. When cells grow exponentially, timer behavior is not able to produce a size homeostasis [6].

Previous studies have studied cell growth behavior in a variety of different organisms. Cladart *et al.* show evidence for near-adder behavior in organisms such as *E. coli*, *S. cerevisiae*, and mamalian cell lines, but Facchetti *et al.* show size control via sizer mechanisms in budding yeast via inhibitor dilution [10].

Biological Relevance of Cell Size Control

Cells are incredibly diverse in size and shape, ranging from 1-2μm in the case of *E. coli*, and up to several hundred mm in the case of axons [34]. This diversity in size and shape has a sizable impact on biological function. A breakdown of cell size control is often associated with cancer, leading some to diagnose cancer based on abnormal cell shape alone [7]. Some cells must drastically change shape in response to their environment. Cell morphology is an important problem to study that affects basic biological function.

1.7   Conclusion

How cells control the size and shape of both themselves and their organelles is an important and long-standing question in Biology. This dissertation will focus on how to measure fluctuations in *Chlamydomonas* flagella as a way to study organelle size control, and how to image the giant ciliate *Stentor coeruleus* as a way to study cell size control mechanisms.

Chapter 2

Biological Noise in Organelle Size Control

David Bauer, Kimberly Wemmer Wallace Marshall

2.1 Abstract

Stochastic variations (noise) in gene expression have been extensively characterized, but the ramifications of this gene-level variation for cellular structure and function remain unclear. To what extent are cellular structures subject to noise? We show that flagellar length in *Chlamydomonas* exhibits significant variation that results from a combination of intrinsic fluctuations within the flagella and extrinsic cell to cell variation. Cells with greater differences in their flagellar lengths show impaired swimming but improved gliding motility,

raising the possibility that cells have evolved mechanisms to tune intrinsic noise in length. We analyzed a series of candidate genes affecting flagella and found that intrinsic noise is increased in mutations which increase the average flagellar length, an effect that can be explained using a theoretical model for flagellar length regulation. Taken together our results show that biological noise exists at the level of subcellular structures, with a corresponding effect on cell function.

2.2   Introduction

Although living cells are often compared to machines, cells are far more dynamic andvariable than man-made machinery. For example, stochastic variation (noise) is well documented in gene expression (Elowitz et al, 2002; Raser et al, 2004; Kaern et al., 2005), and the biological influence of this variation remains a topic of great interest. Random fluctuations in gene expression, regulatory state, or cell behavior might simply represent uncontrollable perturbations that cells try to suppress, but they could also be part of a strategy by which cells cope with a randomly changing environment (Perkins and Swain, 2009). At the level of the whole cell, structure and function are influenced by the joint action of dozens or hundreds of individual genes. It is not obvious a priori how the independent fluctuations in the genes contributing to a given biological process would interact as one goes from the level of single genes to larger scales of intracellular function and organization. We therefore quantified the level of noise in biological structure at the cellular level by examining

stochastic variations in the length of the eukaryotic flagellum, an organelle chosen for these studies because of its simple geometry. Cilia and flagella are interchangeable terms for the microtubule-based organelles that project from the surface of most eukaryotic cells (Pazour and Rosenbaum, 2002) and perform important motile and sensory functions (Scholey and Anderson, 2006). Because these organelles are simple linear structures, it is easier to analyze the length regulation of cilia and flagella than it is to analyze size control in more complicated organelles. The flagellum is thus an excellent test-bed for exploring the systems biology of cellular structure (Randall, 1969; Wemmer and Marshall, 2007). The lengths of cilia and flagella are known to vary from cell to cell in a variety of organisms (Randall, 1969; Wheatley and Bowser, 2000; Adams et al., 1985) suggesting these organelles can be used to analyze biological noise at the level of cellular structure.

2.3   Results

Flagellar length control system exhibits both extrinsic and intrinsic noise

In order to analyze noise in flagellar length, we measured lengths in the unicellular green alga *Chlamydomonas reinhardtii* (Merchant et al., 2007), a well established model organism for the study of cilia and flagella. Each *Chlamydomonas* cell has two flagella approximately 10 μm long (Fig 2.1A inset). This organism has long been used in studies of flagellar length

control because its flagella are easy to measure and because mutants exist in which flagellar length is altered (Wemmer and Marshall, 2007).

Our quantitative analysis of noise in flagellar length is based on approaches previously developed for gene expression analysis. Two distinct types of noise have been described for studies of gene expression: extrinsic noise, which describes the variation in overall expression levels from cell to cell, and intrinsic noise which describes variations in transcription rates at an individual promotor (Elowitz et al, 2002; Raser et al., 2004). In gene expression studies, the distinction between the two types of noise is measured using a dual-reporter method (Elowitz et al., 2002), in which two different fluorescent protein reporter constructs are driven by identical promotors, so that variation in expression of both constructs can be measured on a cell-by-cell basis. The ability to distinguish between fluctuations within a single gene from variation that is shared by the whole cell has been critical to understanding the mechanisms and functional implications of transcriptional noise.

We are able to distinguish intrinsic and extrinsic noise in the case of flagellar length, by exploiting the fact that *Chlamydomonas reinhardtii* cells naturally have two identical flagella. We measured the lengths of both flagella in a population of cells (see Fig 2.1A) and from these data we computed the intrinsic and extrinsic noise using the same mathematical definitions used for gene expression studies (See Materials and Methods).

As shown in Fig 2.1A, and summarized in Table 2.1, flagellar lengths in wild-type cells demonstrated measurable levels of both intrinsic and extrinsic noise. Intrinsic noise describes the variations in length between the two flagella within one cell and may represent
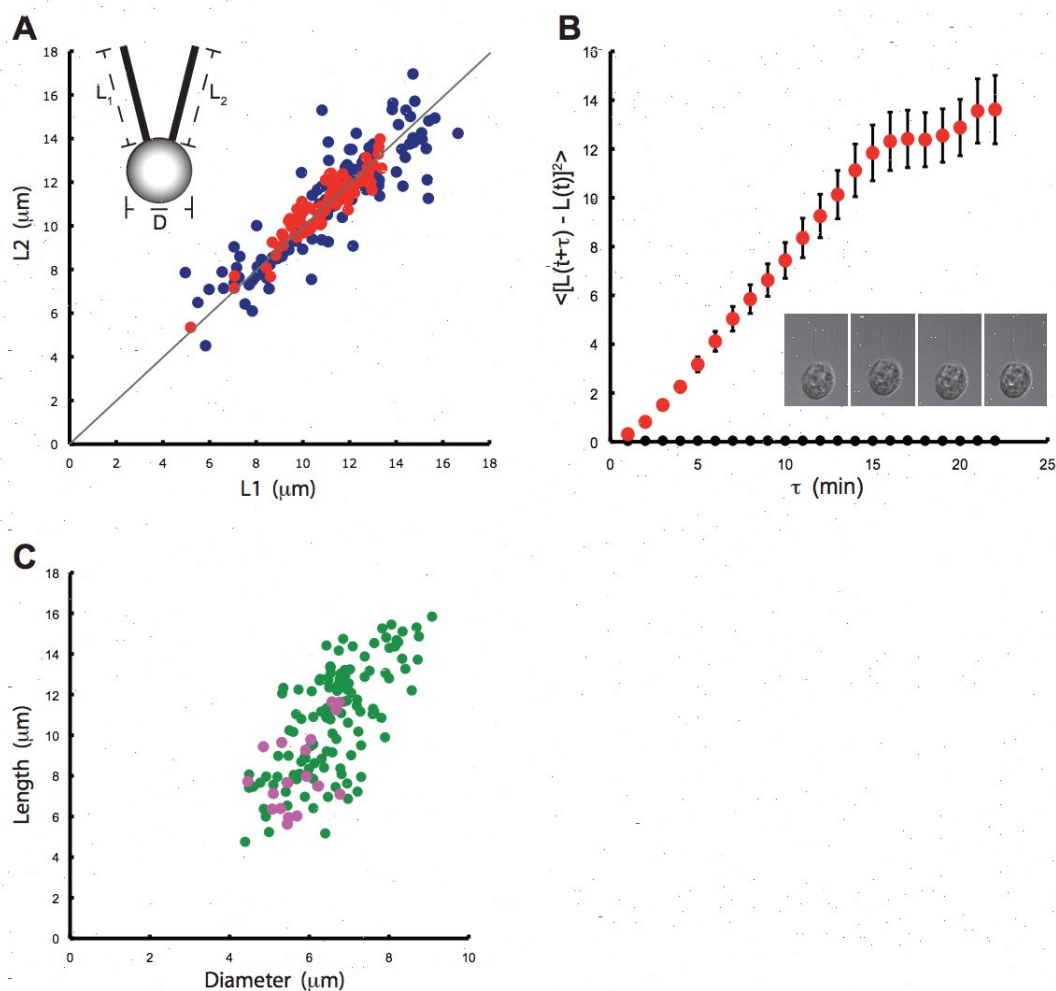
Figure 2.1: Measuring intrinsic and extrinsic noise in the flagellar length control system. (A) Intrinsic and extrinsic noise can be visualized in measurements of flagellar length in fixed *Chlamydomonas* cells with two equivalent flagella. Graph plots length of one flagellum versus length of the other flagellum. Extrinsic noise is reflected by scatter along the diagonal $L_1 = L_2$ (gray line). Intrinsic noise is reflected by scatter perpendicular to this axis. (Blue) wild-type asynchronous culture, (Red) wild-type gametes. (Inset) Cartoon of a *Chlamydomonas* cell showing the three measurements reported in this paper. (B) Fluctuations in length observed in living cells. (Red) Mean squared change in length plotted versus time, showing constrained diffusion-like behavior. Error bars signify standard error of the mean. (Black) Mean squared change in length in glutaraldehyde-fixed cells as an indicator of measurement error. (Inset) Four successive time points of a 3D time series of a single living cell embedded in agarose and imaged with DIC microscopy, similar to the images used to generate the data in this plot. (C) Contribution to extrinsic noise from cell size variation measured by correlation between length with cell diameter in asynchronous cultures. (Green) Wild-type cells. (Pink) *mat3* mutant cells that have smaller average size than wild-type (Umen and Goodenough, 2001) were used to extend the available size range for analysis. Correlation coefficients were 0.61 for wild-type cells alone and 0.70 for the combination of wild-type cells plus *mat3* cells.

Table 2.1: Table 1. Summary of noise calculations. $\langle L \rangle$ denotes average flagellar length in μm, with standard deviation listed. $\langle D \rangle$ is the average cell diameter in μm. r is the correlation coefficient between flagellar length and cell diameter. Noise measures η^2 listed are the actual measurements multiplied by 100. n is the number of cells measured.

Strain	$\langle L \rangle$	$\langle D \rangle$	r	η^2_{int}(x10^{-2})	η^2_{ext}(x10^{-2})	n
Asynchronous cultures						
wt	11.1±2.7	6.8± 0.9	0.61	0.73(0.54-0.95)	5.0(4.0-6.1)	105
lf1	13.8±6.9	6.1±1.2	0.27	13.5 (9.1-18.7)	10.8 (6.9-15.0)	141
lf4	17.8±7.4	6.2±1.2	0.22	1.5 (0.92-2.08)	15.6 (11.4-20.0)	88
Cell-cycle arrested						
wt (dark)	9.9±0.9	6.2±1.0	0.75	0.32 (0.25-0.41)	0.57 (0.38-0.78)	70
wt (gamete)	10.9±1.4	5.2±0.7	0.07	0.12 (0.09-0.15)	1.6 (1.0-2.3)	92
lf1 (gamete)	13.9±5.7	4.5±0.9	0.36	2.2 (1.1-4.2)	12.2 (5.8-18.3)	18
lf4 (gamete)	23.5±8.4	5.2±0.7	0.06	1.8 (0.57-3.7)	10.8 (3.6-20.9)	22
Functional selection						
fast divers	11.1±1.2	6.1±1.0	0.51	0.42 (0.25-0.64)	0.73 (0.51-0.94)	106
slow divers	9.4±2.4	6.0±1.0	0.39	2.9 (1.7-4.4)	3.6 (1.8-5.7)	108

<center>95</center>

fluctuations within the length-control machinery intrinsic to each flagellum, while extrinsic noise describes the cell to cell variation in length and may represent fluctuations in cell-wide features such as cell size (see below). We found that the extrinsic noise is greater in magnitude than the intrinsic noise. The intrinsic noise is, however, significantly greater than the estimated measurement error (see Materials and Methods), thus we can conclude that flagella are subject to biological noise.

Fig 2.1A depicts variation in flagellar length in a population of fixed cells. Does this variation reflect stable differences between cells or random fluctuations over time within individual cell? To answer this question, we embedded cells in agarose and acquired time-lapse

3D movies using DIC microscopy. A plot of the mean-squared change in flagellar length as a function of time-interval (Fig 2.1B) shows that flagellar lengths appear to undergo diffusive dynamics at short time scales, with a mean squared length change linearly proportional to the time interval. At longer time-scales, the mean squared length difference reaches a plateau suggesting that the magnitude of the length variation is constrained. This constraint on length variation indicates the existence of a flagellar length control system, whose molecular basis remains largely unknown (Wemmer and Marshall, 2007).

We next investigated the source of extrinsic noise. Extrinsic noise in gene expression is dominated by variation in cell size (Raser et al., 2004), presumably because larger cells have more ribosomes thus making more protein per mRNA molecule. Flagellar length depends on the availability of flagellar precursor proteins (Rosenbaum et al., 1969; Coyne and Rosenbaum 1979), suggesting that larger cells might have longer flagella due to increased numbers of ribosomes. Indeed, it has been noted that larger cells sometimes have longer flagella in various mutants (Adams et al., 1985). We found that extrinsic variations in flagellar length, as quantified by the average of the lengths of the two flagella in a given cell, was strongly correlated with cell size (Fig 2.1C). Extrinsic noise can also result from variations in cell cycle state. We compared noise in asynchronous cultures (which were used to obtain the data discussed above) to noise in cells arrested in G1 by growth in the dark in minimal media, and to gamete cultures which are arrested in a G0-like state in preparation for mating. Extrinsic noise was significantly reduced by both types of cell cycle arrest (Table 2.1), suggesting that cell-to-cell variations in cell cycle state contributed to increased extrinsic

noise in the asynchronous cultures. As shown in Table 1, the correlation between cell size and flagellar length is stronger in G1 arrested cells (r=0.75) than in asynchronous cultures (r=0.61) suggesting that when variation due to cell cycle progression is eliminated, the remaining extrinsic noise is more closely determined by cell size variation.

Decomposition of total noise into intrinsic and extrinsic components requires that the extrinsic component must vary on a time scale that is long compared to the intrinsic fluctuation time scale (Hilfinger and Paulsson, 2011). *Chlamydomonas* cells grow and divide on a time scale of many hours, while flagellar length changes such as flagellar growth and resorbtion occur on a time scale of tens of minutes, hence the delineation of intrinsic and extrinsic noise is justified on this basis.

Biological relevance of intrinsic length noise

In order to investigate the biological significance of noise in flagellar length control, we asked whether intrinsic noise (i.e. inequality in flagellar lengths) affects flagella driven motility. *Chlamydomonas* cells bend their two flagella in opposite directions in order to swim forward in a breast-stroke like motion. Inequality in lengths due to intrinsic noise might thus be expected to prevent a cell from swimming forward effectively in a straight line. To test this prediction, we observed *Chlamydomonas* cells swimming using a high speed camera, and measured the lengths of both flagella as well as swimming speed. As shown in Fig 2.2A, we found that optimal swimming occurred when both flagella were of approximately equal length

and when their lengths were in the range 8-12 microns. Outside of this range, swimming speed decreased dramatically. The defects in swimming were different depending on the type of length variation. When both flagella were too long, the extra length of flagellum appeared to flail ineffectively through the media, presumably impeding forward progress. On the other hand, if both flagella were too short, they were unable to generate an asymmetrical bending motion. Consequently, the flagella just move back and forth but could not create overall forward motion because symmetrical swimming movements do not produce motion at low Reynolds number. If the two flagella were of sufficiently unequal length, the cells swam in circles. These results indicate that to the extent that a length control system may have evolved to ensure effective swimming, it must satisfy two goals: ensure equality of flagellar length within a cell, and ensure that the two flagella are in roughly the right average length range.

We next compared the actual distribution of flagellar lengths to the range of flagellar lengths that gives optimal swimming efficiency. As indicated by the dots in Figure 2A, wild-type cells have a joint distribution of lengths for their two flagella that corresponds to the optimal range of flagellar lengths for fast swimming. Thus, any increase in noise that would lead to variation outside this range would decrease swimming fitness. The joint length distribution in gametes matches the region of optimal swimming even more closely (Figure 2 - Figure supplement 1) due to the lower intrinsic noise in gametes.

Although flagella are used for swimming when cells are in suspension, they can also generate gliding motility when cells are adhered to a solid substrate (Bloodgood 1981). Gliding
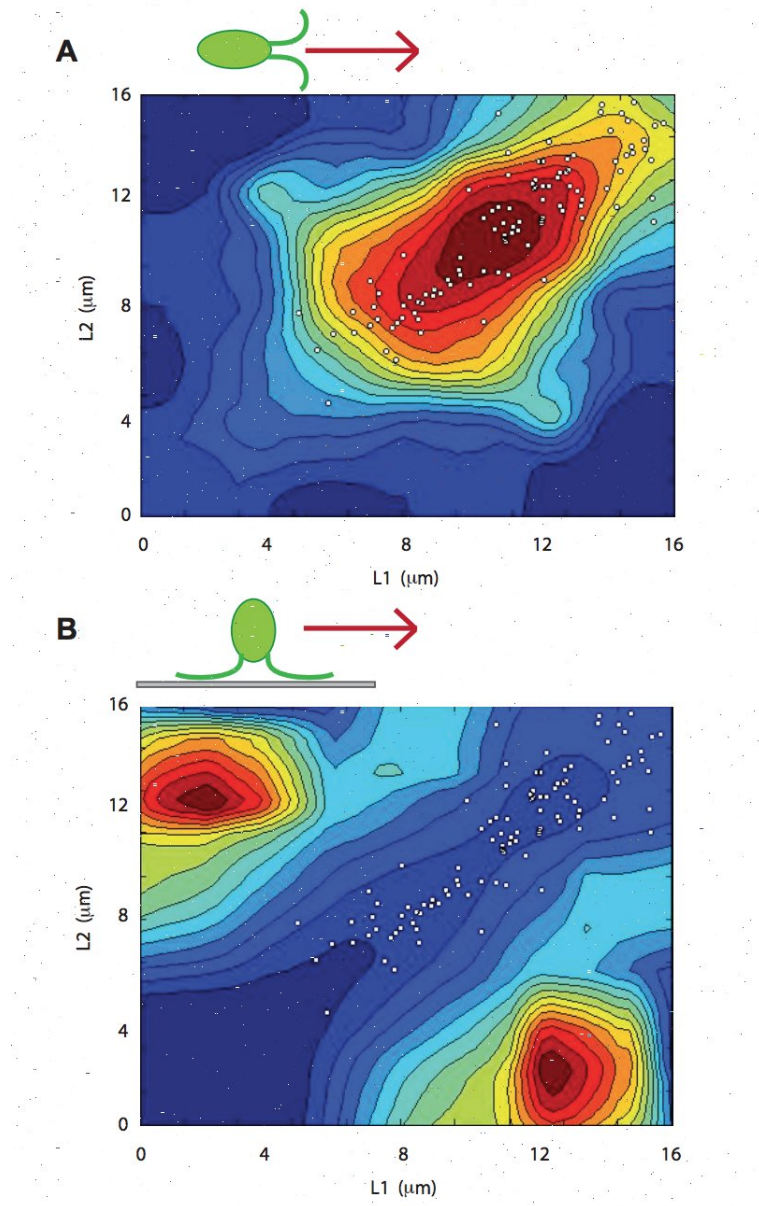
Figure 2.2: Noise affects fitness as judged by flagella-driven motility. (A) Contour plot of swimming speed (red fastest, blue slowest) versus the lengths of the two flagella. White dots signify lengths of flagella in wild-type cells superimposed on swimming speed distribution. (B) Contour plot of gliding speed (red fastest, blue slowest) versus the lengths of the two flagella.

is an important type of motion for a soil-dwelling alga and one that is thought to possibly have evolved prior to bending-type flagellar motility required for swimming (Mitchell, 2007). Gliding involves motion of transmembrane proteins in the flagellar membrane adhering to the surface and then being pulled by a Kinesin- and Dynein-dependent motile process known as intraflagellar transport (IFT) (Shih et al., 2013). Does flagellar length variation affect gliding motility in a similar way to its effects on swimming motility? To answer this question we imaged live cells during gliding using DIC microscopy and measured their flagellar lengths and gliding speeds, assessed as the distance the cell travelled over a fixed period of time (see Materials and Methods). The results of this analysis (Fig 2.2B) were strikingly different from those of the swimming speed analysis. Unlike swimming, which was fastest when the two flagella were of equal length, gliding was fastest when the two flagella were of unequal length (correlation coefficient between length difference and gliding velocity r=0.52, n=141, $p < 10^{-7}$). Gliding velocity correlated with the difference in the lengths of the two flagella, but not with the average of the two flagella (r=-0.014), confirming prior reports that overall flagellar length did not influence gliding speed (Bloodgood, 1981). Gliding thus appears to be sensitive to intrinsic noise affecting the length of one flagellum versus the other, but not extrinsic noise affecting both flagella. We noted that in gliding cells with unequal length flagella, cells always moved in the direction of the longer flagellum. We hypothesize that this behavior might reflect the tug-of-war nature of gliding motility (Shih et al., 2013) such that one flagellum can only glide if the other flagellum is not gliding. In cells with equal length flagella, we would therefore expect to see the cell jitter back and forth rather than undergo

long periods of directed movement, and indeed this is the case. As shown in Supplementary Fig 2.7, we find that the frequency of reversal of gliding direction is highest in cells that have equal length flagella (r=-0.35 between length difference and reversal frequency, p=10^{-5}). Cells in which one flagellum is much longer than the other show a low frequency of directional reversal, and tend to move at high speed in the direction of the longer flagellum. A more extreme form of this observation was previously reported by Bloodgood, who observed that cells in which one flagellum had been sheared off always glided in the direction of the remaining flagellum and did not undergo any directional reversals (Bloodgood, 1981).

The fact that flagellar length inequality is beneficial for gliding but deleterious for swimming suggests that the increased intrinsic noise in vegetative cells compared to gametes may represent a form of bet-hedging, allowing vegetative cells to exploit both types of motility. Gametes are optimized for mating, a process that requires opposite mating type cells to swim together and pair through their flagellar tips, and therefore they may have evolved stricter control over intrinsic noise to optimize these specific behaviors.

The hypothesis that intrinsic biological noise can have both positive and negative effects on fitness raises the possibility that particular genes may have evolved to regulate intrinsic noise.

Identifying genes that regulate noise in flagellar length control system

We therefore used our noise measurement assay to test a panel of candidate genes and cellular processes for possible roles in noise suppression (Fig 2.3A). First we asked whether transcription or translation were needed to actively regulate intrinsic noise. In cells treated with cycloheximide as previously described (Rosenbaum et al., 1969), intrinsic noise was not significantly altered compared to untreated cells. We also ruled out a role for hydrodynamic coupling between the two beating flagella by showing that paralyzed mutants *pf15* and *pf18* had no increase in noise.

Since the two flagella are physically associated at their basal bodies, we speculated that this connection might help coordinate flagellar dynamics between the two flagella and thereby reduce intrinsic noise. We therefore analyzed *asq2* mutant cells, which we have previously shown to be defective in the physical connections between mother and daughter basal bodies (Feldman et al., 2007). However, the *asq2* mutation had no effect on intrinsic noise, nor did the *vfl2* mutation which lacks fibers that normally connect the basal bodies to the nucleus (Wright et al., 1985).

We next examined mutants with altered flagellar length. Mutations in the SHF1, SHF2, and SHF3 genes have been reported to cause cells to form short flagella, roughly half wild-type length. Noise measurements in these mutants did not show any increase in intrinsic noise. In contrast, we saw a dramatic increase in intrinsic noise in *lf1*, *lf2*, *lf3*, and *lf4* mutants,
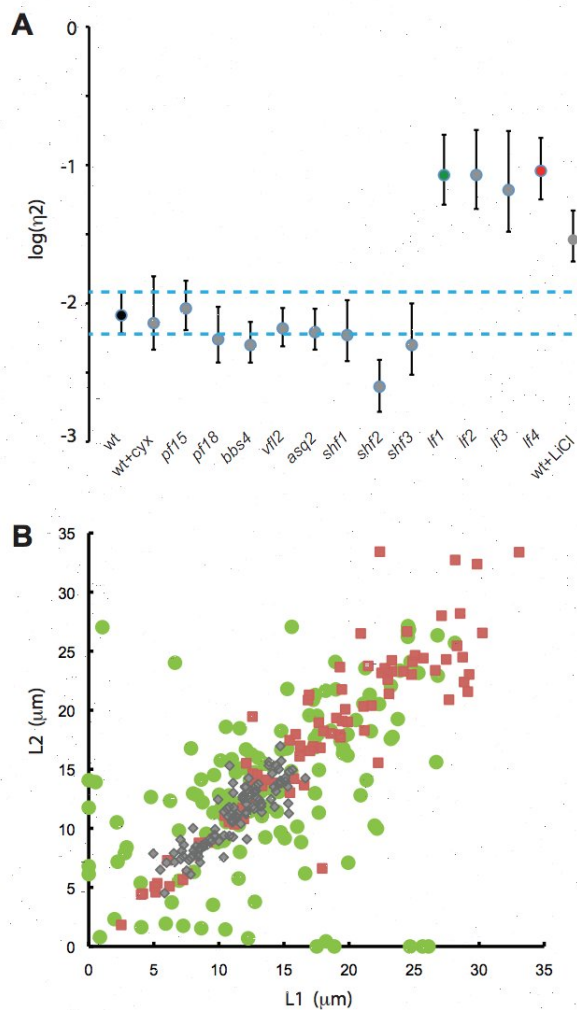
Figure 2.3: Identification of genes that participate in flagellar length noise suppression. (A) Analysis of candidate genes for effect on noise. Points represent median intrinsic noise. Error bars are 95 percent confidence intervals for each strain. Dotted blue lines show the 95 percent confidence interval for intrinsic noise in wild-type cells. Green and Red data markers indicate *lf1* and *lf4* mutants. All measurements were made using 2D image data to allow a large number of different strains to be measured more rapidly. (B) Increased intrinsic and extrinsic noise in long flagella mutants. (Green circles) *lf1*, (Red squares) *lf4*, (Gray diamonds) wild-type. All data shown is from 3D measurements of flagellar length in cells from asynchronous cultures.

all of which have abnormally long flagella (McVittie, 1972; Barsel et al., 1988; Berman et al., 2003; Nguyen et al., 2005; Tam et al., 2007). This suggested that increased length might somehow cause increased intrinsic noise. To confirm this hypothesis, we measured noise in wild-type cells treated with lithium, which increases flagellar length (Nakamura et al., 1987). As with the *lf* mutants, we found that lithium treated cells also showed increased intrinsic noise in flagellar length. Taking these data together, we conclude that the LF genes appear to play a role in regulating noise, while neither the SHF genes, transcription, translation, flagellar motility, nor basal body connections play a significant role in noise control.

To further examine the role that LF genes play in noise regulation, we examined individual mutants in more detail. Fig 2.3B plots the distribution of flagellar length pairs in *lf1* and *lf4* mutants. Both mutants cause the average flagellar length to be approximately double wild-type length. It was previously reported that the *lf1* mutation leads to increased variance in length (McVittie, 1972) but in that analysis no attempt had been made to distinguish intrinsic and extrinsic variation. As indicated in Fig 2.3B, we found that both mutations lead to increased noise, but in different ways: *lf1* mainly increases intrinsic noise while *lf4* increases both types of noise (Table 2.1). This suggests the two genes act in fundamentally different ways within the length control system, with the LF4 gene product acting to cell-to-cell variation in length and the LF1 gene product acting to promote equality in length of the two flagella within a cell regardless of their average length. For both mutants, the quantitative effect of the *lf* mutations on noise is much greater than their effect on average length (Table 2.1), suggesting that the LF gene products may have evolved primarily as a

means to restrain length variation, as opposed to setting any particular average length.

The increase in extrinsic noise (cell to cell variation) in the *lf4* mutant raises two alternative possibilities for the function of the LF4 gene. One possibility is that LF4 is involved in constraining cell size, such that the *lf4* mutant would have a wider variation in cell body size thus leading to a larger variation in cytoplasmic precursor production and thereby an increase in the level of extrinsic noise. It is indeed the case that the standard deviation in cell diameter increased slightly in *lf4* compared to wild-type, by a ratio of 1.3. However, the increase in cell size is far less than the increase in standard deviation in flagellar lengths, so increased cell size variability is unlikely to be the sole explanation for the increased extrinsic noise in *lf4*. The other possibility is that the *lf4* mutation may cause length to depend more strongly on cell size than in wild-type. This possibility is supported by the fact that the slope of the best-fit line relating flagellar length to cell diameter increases from 0.96 in wild type to 1.74 in *lf4* cells. We do not currently know how to explain this steeper dependence of flagellar length on cell diameter in *lf4* mutants compared to wild-type.

In summary our analysis of noise in Chlamydomonas mutants revealed that LF1 and LF4 genes act to reduce biological noise in flagellar length. In fact, both genes seem to have a larger effect on noise than they do on the average flagellar length, suggesting that noise suppression may be their primary evolutionary purpose.
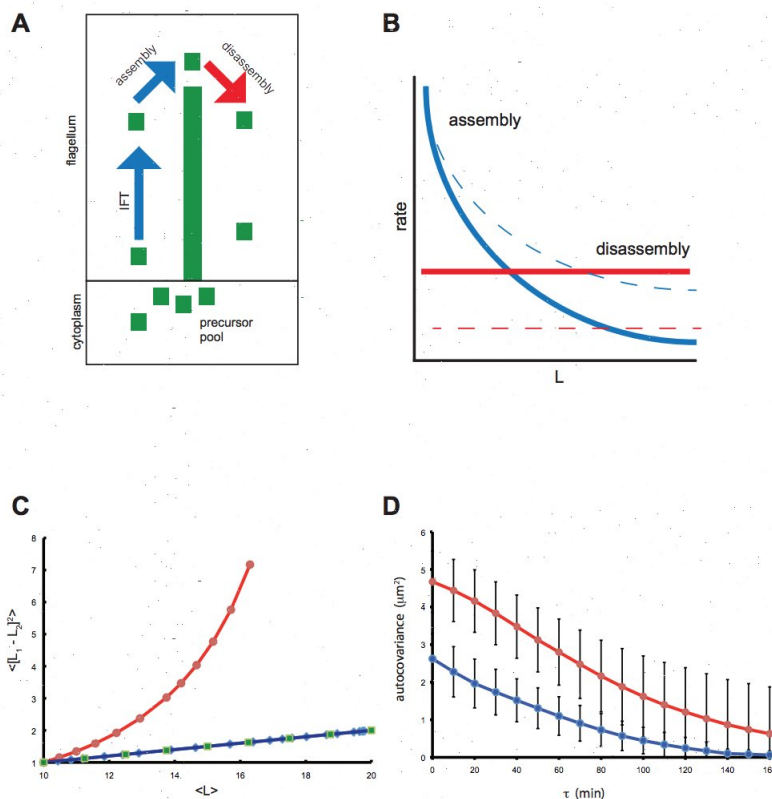
Noise analysis of balance-point model for flagellar length control

The noise measurements reported here provide a new way to test hypothetical flagellar length control system models, since any model for such a system must be able to account for not only the average steady-state behavior of the system, but also the fluctuations that occur within the system. Any model that claims to explain flagellar length control must therefore be able to account for the observation presented above that mutations leading to increased average length also lead to increased intrinsic noise.

We have previously described a model, outlined in Fig 2.4A and B, for flagellar length control (Marshall and Rosenbaum, 2001; Marshall et al., 2005), based on the intrinsic length-dependence of intraflagellar transport (IFT). IFT is mediated by the kinesin-driven movement of protein complexes called IFT particles which bind to and transport tubulin and other flagellar buiding blocks out to the flagellar tip, where they assemble into the growing structure (Qin et al., 2004; Hao et al., 2011; Bhogaraju et al., 2013). Our IFT-based length control model contains three parameters, A, D, and P, which represent the efficiency of IFT, the rate of disassembly at the tip, and the level of flagellar structural protein synthesized by the cell. As previously derived (Marshall and Rosenbaum, 2001) and explained further in Materials and Methods, the steady-state average flagellar length for this model is:

$$\langle L \rangle = \frac{P}{2 + \frac{D}{A}} \tag{2.1}$$

Clearly, average length can be increased either by increasing A, increasing P, or decreasing D. How would length-increasing parameter changes affect noise? To answer this question

Figure 2.4: Noise analysis of a length control system model. (A) Schematic of balancepoint mode for flagellar length control. Flagellar microtubules undergo constant disassembly (red arrow) at a length-independent rate D. This disassembly is balanced by assembly, which occurs at a rate limited by the rate of IFT (blue arrow). Assuming the number of IFT particles is length-independent, the rate of cargo delivery at the tip is proportional to 1/L. Precursor protein from the cytoplasm binds with first order binding. The available free precursor pool is the total pool P minus the quantity of precursor already incorporated into the two flagella. Hence the net assembly rate is given by A(P2L)/L. (B) Steady-state length is determined by the balance point between length-independent disassembly (Red line) and length-dependent assembly (Blue line). Mutations can increase flagellar length either by increasing assembly (Blue dotted line) or decreasing disassembly (Red dotted line). (C) Results of small signal noise analysis . Plot shows the mean squared difference in the lengths of the two flagella plotted versus their average length, while parameters A (describing the efficacy of IFT), D (describing the rate of steady state axoneme disassembly), or P (describing the total pool of flagellar precursor protein) are changed so as to increase length from 10 to 12 microns. (Red circles) results of decreasing D, (Blue diamonds) results of increasing A, (Green squares) results of increasing P. Since the strength of the noise source is not known, all results are normalized to a value of 1 at the wild-type length of 10 microns. Parameter values for the wild-type case are those previously derived from experimental measurements (Marshall and Rosenbaum, 2001). (D) Autocovariance of *lf1* (red) versus wild-type (blue) based on measurements of length fluctuations in living cells, showing higher mean squared fluctuations (based on autocovariance at zero lag) and slower decay for *lf* mutants, as predicted by the linear noise model.

we have performed a small-signal linear noise analysis as derived in Materials and Methods. We do not know the ultimate source of intrinsic noise in this system, but we postulate that it may result from random fluctuations in the growth rate at the tip. Growth rate fluctuations would cause the length to execute a one-dimensional random walk, with the length-dependent growth and shrinkage rates created by the balance point model providing a restoring influence that returns the length back to its set point after any fluctuation. Modeling flagellar length fluctuations is thus analogous to the classical problem of modeling the Brownian motion of a particle attached to a spring. In our case the noise source is due to random variation in assembly rates at the tip rather than thermal collisions, and the Hookean restoring force is a consequence of the fact that we use a linearized model to describe the rate of length change as a function of displacement from the stead-state solution. Under our assumptions, as derived in Materials and Methods, length noise is predicted to depend on model parameters as follows:

$$\langle (L_1 - L2)^2 \rangle \sim \frac{P}{D[2 + \frac{D}{A}]} \tag{2.2}$$

Results predicted by Equation 2.2 are plotted in Fig 2.4C. Note that any parameter change that increases flagellar length is predicted by Equation 2.2 to result in increased intrinsic noise, but changes in different parameters can have different relative effects on intrinsic noise. Changing either the cytoplasmic precursor pool size or the IFT efficacy have almost identical effects on noise, and in both cases the increase in the mean squared difference in the length of the two flagella (intrinsic noise) is linearly proportional to the increase in length, so a

mutation that causes a doubling of average length should cause approximately a doubling of mean squared length differences. In contrast, changes to the disassembly rate D have a much larger, non-linear effect. It may thus be possible to predict which parameters of the model are affected by particular mutations, by determining the extent to which each mutation increases noise relative to average length. Thus, the first prediction of this model is that any parameter change that leads to an increase in length should also increase intrinsic noise in the balance-point length control system. A second prediction of this model, derived in Materials and Methods, is that the effect of fluctuations will be less quickly damped out in mutants with long flagella. Indeed, the reason that the variance in length is predicted to increase in this model is that the effect of individual fluctuations should damp out more slowly in long-flagella mutants. This allows multiple fluctuations to add up to produce larger deviations from the average solution. The reason that fluctuations damp more slowly in long-flagella mutants relates to the shape of the assembly versus length curve in the balance-point model (Fig 2.4B). Considering only small fluctuations, the rate at which any given fluctuation is corrected is roughly the product of the magnitude of the fluctuation and the slope of the assembly-versus-length curve in the region of the steady-state solution, since the disassembly curve is a horizontal line. Since the assembly versus length curve is an hyperbola, its slope is a continuously decreasing function of length. For long flagella obtained via a decrease in disassembly rate, such mutants will have a decreased slope of their assembly curve at the steady state solution, thus fluctuations will persist for longer than wild-type. For long flagella obtained via an increase in either the precursor pool size or the efficacy of IFT, the

length dependence of the assembly curve would be re-scaled to produce a lower slope at every value of length, again leading to slower damping of fluctuations.

In order to determine if the increased intrinsic noise in *lf1* mutants was due to larger dynamic fluctuations, we analyzed fluctuations in individual *lf1* mutant cells using timelapse microscopy. As shown in Figure 4D, we found that the fluctuation magnitude of individual flagella was approximately double in *lf1* compared to wild type (as judged by the autocovariance value for zero lag). This is the same order of magnitude increase as predicted by the theoretical noise model for mutations affecting either IFT or cytoplasmic precursor pool size, but would not be consistent with an alteration in disassembly rate. Moreover, the fluctuations were damped out more slowly in *lf1* compared to wild-type as judged by the decay of the autocovariance function, in full agreement with the model. A best fit exponential to the data of Fig 2.4D indicated a decay time constant of 101 min for wild-type and 183 min for *lf1*. We conclude that the balance-point model can predict the observed increase in intrinsic noise seen in *lf* mutants.

Microfluidcs enable single cell extrinsic noise measurements

We interpret extrinsic noise as noise existing in the cell, which influences flagellar length. If there are sources of variation contained in the cell body, outside of the flagella, then those sources of variation can in principle be identified by removing the flagella and having the cell regenerate new flagella. As long as the variation in cells takes place on a slow timescale rel-

ative to the time required for flagellar regeneration, we should observe a correlation between flagellar length before and after regeneration. However, conventional protocols for flagellar regeneration are done in suspended cultures, making it impossible to relate flagellar length prior to flagella shedding with flagellar length after regeneration. In order to investigate to what extent extrinsic noise is present in the flagellar length circuit, we built a microfluidic device capable of trapping *Chlamydomonas* cells with solution exchange. An image of the device can be seen at Supplementary Fig 2.8. A single device is capable of immobilizing approximately 100 cells to a narrow z-plane (15 μm). The trapped cells are stable for many hours (>24), undergo cell division, and regenerate flagella. With this device, we are capable of taking an initial flagellar length measurement, pH-shocking the cell to induce flagellar regeneration, and then making a final flagellar length measurement. This allows us to evaluate how reliably a cell can rebuild its flagella, and provides us with a system to estimate the extrinsic noise. Flagellar regeneration experiments (described in section 2.6) indicate that there is extrinsic noise present in the *Chlamydomonas* length control. We find that the final length (mean 8.5 μm) is not equal to the initial length (10.0 μm) (p$\ll$0.01), as seen in Fig 2.5B. These results are consistent with prior reports (Rosenbaum et al., 1969) that regrowth of flagella is not fully completed by 120 minutes. This result for the extrinsic noise (1.5 μm) is somewhere in between an asynchronous and arrested culture. Initial and final length were correlated with r=0.38 (p$\ll$0.01), suggesting a significant influence of a cell-body associated factor with flagellar length. One possible source of the cell-body linked extrinsic noise could be cell size, in that larger cells tend to have longer flagella. Dominance analysis (Budescu
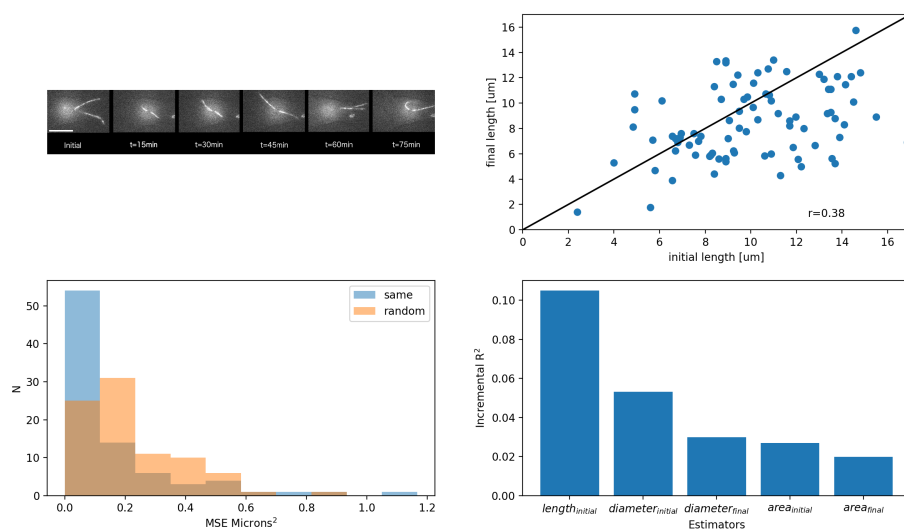
Figure 2.5: An example of a flagellar regeneration sequence in the microfluidic device. A max-z projection is shown for the initial length, and for 15-minute increments after the pH shock. The scale bar represents 5 μm. b) A scatter plot of the initial (x-axis) and final (y-axis) lengths. Each point represents a pair of before and after pH shock length measurements from a single cell. Each cell can have up to two points. The black diagonal line represents $y = x$. c) Histogram comparing mean squared errors of initial - final length measurements. (blue) The MSE of flagella belonging to the same cell. (orange) The MSE length measurements where the initial and final length are from two different, randomly chosen cells. The means of the two distributions are 0.15 μm^2 and 0.22 μm^2 (p≪0.01) for the same cell and randomly chosen cell distrubutions, respectively.) e) Results of dominance analysis. Plot shows the incremental r^2 contribution of each predictor in the model.

et al., 1993) indicates that after performing multiple regression on the final length vs initial length, initial cell diameter, initial cell area, and final cell area, the initial length accounts for the greatest proportion of the variance (45% of total), shown in Fig 2.5D. Additionally, initial length (r=0.38, p≪0.01) has a stronger correlation than initial diameter (r=0.31, p=0.004), or final diameter (r=0.23, p=0.04). We conclude that flagellar length is subject to extrinsic noise present in the cell body, and that the source of this cell-cell variation is likely not accountable purely by cell size variation.

2.4   Discussion

The results presented here show that the flagellar length control system in *Chlamydomonas reinhardtii* exhibits both intrinsic and extrinsic noise. The overall effect of these noise sources is that in a wild-type cell, the coefficient of variation (standard deviation in flagellar length divided by average flagellar length length) is in the range 10-20%, which is comparable to the measured variability in length of vertebrate cilia (Wheatley and Bowser, 2002) and in the length of bacterial flagellar hooks (Koroyasu et al., 1998). While it is commonplace to compare cells and cellular structures with man-made machines, such a high level of size variability would not be tolerated in most manufacturing processes. It is therefore interesting to consider whether the level of noise that is observed indicates that cells cannot do any better, or alternatively that the noise serves an optimized function, such as jitter in mechanical devices. The close alignment between the distribution of flagellar lengths in wildtype cells and the length range for optimal swimming speed (Fig 2.2) strongly suggests that the latter explanation is correct — there is no evolutionary pressure to reduce variability in flagellar length below a level that is tolerable for effective swimming. In fact, quite to the contrary, there appears to be an evolutionary pressure to maintain some degree of intrinsic noise to allow for better gliding motility. Variability in flagellar length may thus benefit a population of cells by giving the population as a whole more flexibility in dealing with changing environmental conditions.

Additionally, our results show that the dependence of noise on average flagellar length

can in principle be explained by a dependence of the noise damping rate on parameters of the flagellar maintenance system that regulate length. Attempts to use noise measurements to define parameters precisely is currently hampered by the fact that we do not know the ultimate source of the noise. One possibility is that intraflagellar transport may show fluctuations in its rate over time, thus producing random variations in the growth rate at the tip. Other sources of variation could include stochastic fluctuations in cargo loading or transport through the flagellar pore. Future studies using quantitative imaging methods will be necessary to determine which microscopic features of the system correlate with macroscopic fluctuations in length.

The presence of extrinsic noise beyond what cell size alone can explain is suggests a mechanism within the cell body that affects flagellar length. One possible way to probe this mechanism is with mutants with functional length control, but abnormal kinetics. One such mutant is Crescerin, a ciliary microtubule regulator [12]. *Chlamydomonas* with mutated Crescerin have wildtype length, but take 2-3 hours to regenerate flagella. It is possible that whatever signal this cell-body mechanism produces may yield a different result when integrated over a longer period of flagellar regeneration.

2.5 Conclusions

Our results demonstrate that concepts of intrinsic and extrinsic noise are directly applicable to biologically relevant structure and function at the level of organelles, influence cell fitness,

and are under genetic control.

2.6 Materials and Methods

Strains, media, and imaging

All strains were obtained from the Chlamydomonas Genetics Center, Duke University, with the exception of *lf4* mutant strain V13 which was a gift of Greg Pazour, UMASS Medical Center. The *lf4* mutation was confirmed in this strain by PCR (data not shown). For asynchronous culture, cells were grown in 2mL cultures in TAP media (Harris, 1989) under continuous illumination. Cultures arrested in G1 were obtained by growing cells in M1 media for 2 days in continuous illumination and then switching them to continuous darkness for 24 hours. Gametes were grown overnight in M-N media. To measure flagellar length in fixed cells, cells were fixed in 1% glutaraldehyde, and imaged using DIC optics with an Olympus 60x air lens and an air condenser on a DeltaVision 3D microscopy system. Three dimensional data was collected using a 0.2 μm step in the Z-axis. Lengths were then measured by tracing the flagella in three dimensions using the DeltaVision distance measuring function with the multi-segment length calculation method. To measure flagellar length fluctuations in live cells, cultures were grown in TAP media at 21∘C in constant light on a roller drum. For embedding live cells, 1% w/v agarose was melted in TAP media and cooled to 41∘C. A square of Vaseline was made on a glass slide, then 5μL of culture was mixed with 20μL agarose in

TAP within the square. The slide was then inverted over a coverslip, compressing the agarose in TAP into a flat, square pad. The cells were allowed to recover at room temperature in light for 2 hours to overnight, then imaged. The slide was imaged using DIC microscopy on a DeltaVision microscopy system, at room temperature in ambient light. Embedded cells were imaged using a 100x oil immersion lens (NA 1.40 PlanApo) with a z step size of 0.2 microns. One z stack was taken through the entire cell every 10 minutes for 2 hours. The length of the flagella was measured using DeltaVision software.

Computing intrinsic and extrinsic noise

We define intrinsic and extrinsic noise in a purely operational sense by treating the two flagellar length measurements from each cell as though they were two fluorescence intensity measurements in a dual-reporter gene expression noise protocol, and computing intrinsic and extrinsic noise using the relations previously described for gene noise (Elowitz et al., 2002), as follows:

$$\eta_{int}^2 = \frac{\langle (L_1 - L_2)^2 \rangle}{2 \langle L_1 \rangle \langle L_2 \rangle}$$

$$\eta_{ext}^2 = \frac{\langle L_1 L_2 \rangle - \langle L_1 \rangle \langle L_2 \rangle}{\langle L_1 \rangle \langle L_2 \rangle}$$

For each given cell measurement, we arbitrarily defined L_1 as referring to the length of the flagellum whose base was closest to the left edge of the field of view.

Estimation of measurement noise

We used time-lapse imaging to obtain two separate estimates for measurement error. First, as plotted by the black datapoints in Figure 1B, we imaged cells fixed in glutaraldehyde at multiple sequential time points and then calculated the mean squared difference in length. As expected for measurement errors that are uncorrelated with each other, the slope of the best fit line to this data was less than $5\mathrm{x}10^{-5}$, showing that the difference in measured length was independent of time lag. The average value of the mean squared difference in length was 0.0438 square microns, corresponding to an average measurement error of 0.2 microns.

As an alternative measure, we analyzed the fluctuations in live cells and calculated the mean squared change in difference between L_1 and L_2, and plotted this versus time. This plot gave a roughly linear behavior for the first several time points. We then fitted a straight line to the first ten time points and obtained a y-intercept of 0.597. For a one-dimensional random walk (such as that executed by the difference in length between the two flagella), the Y intercept of this plot should correspond to 4 times the mean squared measurement error in each measurement. We therefore obtain an estimated measurement error of 0.39 microns. We thus obtain two independent estimates of measurement error, both of which are on the same order of magnitude as the XYZ voxel size.

Measurement of swimming speed versus flagellar length by high speed video

To obtain simultaneous measurements of swimming speed and flagellar lengths we mounted cells between a slide and coverslip supported by a 1 mm thick Vaseline ring, and imaged the cells on a Zeiss Axiovert 200M microscope with a 40X air objective lens using DIC optics and an infrared-blocking filter, collecting data with a Phantom MiroEx4-1024MM video camera at a frame rate of 1000 fps, exposure time 998 μsec. Cells were imaged at a dilution that ensured at most one or two cells per field of view. Following collection of each dataset, individual cells were manually tracked for 10 cycles of flagellar beating, marking the position of the cell at the beginning and end of this period. The difference in position divided by the elapsed time was taken as the average swimming speed. Since our data collection was only two-dimensional, many cells swam out of focus during the imaging and those images were discarded. Only cells for which the flagella remained in focus through the entire 10 beat cycles were used for distance measurements. Distance measurements of swimming and length measurement of flagella were performed using the Phantom Miro software.

Measurement of gliding versus flagellar length

Cells were grown in TAP media and loaded onto a coverslip within a 2 mm thick Vaseline ring and inverted over a slide. Cells were imaged using a 20x objective with DIC optics. 25 images were collected at a rate of 1 image every 10 seconds. The total distance travelled by

a cell was then calculated as the distance between the start and end point of the time series and the velocity calculated by dividing this distance by the total data collection time. The number of directional reversals for each cell during the entire time-course was determined by visual inspection.

Measuring Extrinsic Noise (Flagellar Regeneration) in a Microfluidic Device

FAP20GFP (ref Yanagisawa et al,. 2014) cells were synchronized via a 14/10 light/dark cycle and hand injected using a syringe and a tube into the device until all traps were occupied. Constant flow was then established by attaching a syringe pump with normal and low-pH M1 media to the loaded device. A valve (Chrom Tech V-100D) was used to switch from normal to low-pH media with minimal lag time. The loaded device was mounted on a custom built OMX (Dobbie et al,. 2011), Leica DMi8, or Nikon Ti-E. All imaging done at 100X. An initial 3D-measurement (16 μm z-stack, axial spacing of 0.2 μm) was taken of flagellar length in the GFP channel (65μW @ 455nm at the sample). Cells were then pH shocked via switching to low-pH media for 60 seconds and returning to normal-pH media. Two hours after pH shock, cells were imaged again in the GFP channel for a final 3D flagellar length measurement. Measurements were made by hand in ImageJ. XY and Z measurements were added in quadrature.

Fabrication and Design of Microfluidic Device

For Design: The device was modeled in Auto-CAD and printed on a plastic transparency film. For Mold: The device was fabricated using standard photo-lithographic methods for a single-layer device. Spin coat a layer of SU8 3010 at 1000rpm. Measured feature height of 15μm. Soft bake at 95∘C for 10 minutes. Expose for $200\frac{mJ}{cm^2}$, then post-exposure bake for 150 seconds. Develop until there is no precipitate upon rinsing in isopropanol. Finally, hard bake 1 hr. For PDMS device: Mix 10:1 monomer to crosslinker Silgard 184. Degas the mixture in a vacuum chamber for 30 minutes, or until air bubbles are no longer visible. Bake at 85∘C for 1.5 hrs. Cut away excess PDMS and punch holes for tubing. For plasma bonding: Place your cover slip and PDMS device in a plasma cleaner, and pull a vacuum. After pressure falls below 0.1 mbar, flow O2 into chamber at 1 mbar. Turn on the RF field for 45 seconds.

Small-signal linear noise analysis of balance-point length control model

We have previously described a simple model for length control of cilia and flagella that has been termed the balance-point model to distinguish it from more elaborate models based on active length sensors (none of which have yet been discovered). The balance point model is based on observations that the axonemal microtubules undergo continuous turnover at their plus-ends, with disassembly taking place at a constant rate regardless of length, and assembly

taking place at a rate limited by IFT (Marshall and Rosenbaum, 2001). A key component of the model is the hypothesis that intraflagellar transport is inherently length-dependent. This dependency arises because the quantity of IFT proteins in the flagellum is independent of flagellar length (Marshall and Rosenbaum, 2001; Marshall et al., 2005). For each IFT particle, moving at a constant velocity, the round-trip transit time is obviously proportional to flagellar length L, hence the frequency with which a particle can deliver protein cargo to the tip is proportional to 1/L. Because the total number of IFT proteins moving in the flagellum is length independent, the overall efficiency by which the IFT system taken as a whole can move proteins out to the tip for assembly is therefore proportional to 1/L. The constant of proportionality depends on the number of IFT proteins in the flagellum, their velocity, etc. Because assembly is rate-limited by transport, it follows that the assembly rate is proportional to 1/L while the disassembly rate is independent of length. Therefore, the assembly rate versus length curve will intersect the disassembly versus length curve at a unique value of the length, which reflects the steady state length of the flagella.

Following our previous formulation of the balance-point length control model, we define three parameters, A, P, and D. Parameter A describes the efficacy of intraflagellar transport and encapsulates the speed of the IFT particles, the number of IFT particles in a flagellum (a quantity known to be independent of length, and the cargo carrying-capacity of the particles. The parameter P describes the total pool of flagellar protein in a cell, including protein incorporated into the two flagella as well as unincorporated precursor stored in the cytoplasm (Rosenbaum et al., 1969). Parameter D describes the rate of flagellar disassembly.

We have previously estimated values for these parameters in wild-type cells: D $\sim$ 0.22 μm/min (measured from the rate of shortening in *fla10* mutant cells), A $\sim$ 0.11 (this is a unit-less quantity), and P $\sim$ 40 μm (measured from the ratio of flagellar lengths before and after regeneration in the presence of cycloheximide (Marshall and Rosenbaum, 2001)). Note that the pool size is expressed in units of length, the conversion factor being the quantity of protein required to assemble a 1 μm segment of the axoneme.

The length control model described in the text can be encapsulated by a pair of differential equations, one for each of the two flagellar lengths L_1 and L_2:

$$\dot{L}_1 = f(L_1, L_2) = A\frac{(P - L_1 - L_2)}{L_1} - D$$
$$\dot{L}_2 = g(L_1, L_2) = A\frac{(P - L_1 - L_2)}{L_2} - D$$

for which the steady state solution is:

$$L_1 = L_2 = L_{ss} = \frac{P}{2 + \frac{D}{A}}$$

With the estimated parameter values given above this predicts a steady state length of 10 μm. Using this model, we would like to predict how changes in the three parameters would affect noise suppression by the system, in order to ask whether parameter changes that increase the steady-state length would be predicted to increase noise. To do this, we employ a linear noise analysis by modeling the response to small perturbations in length. Increased sensitivity to small perturbations would tend to result in a noisier system.

We begin our noise analysis by introducing a change in variables:

$$x = L_1 - L_2$$

$$y = L_1 + L_2 - 2L_{ss}$$

The new variables x and y correspond to the intrinsic and extrinsic noise, respectively, that will result from a fluctuation applied to one of the two flagella. We next consider the effect of applying a small perturbation to L_1 at time $t = 0$. Initially this perturbation would increase both x and y, but then over time the system will restore the flagellar lengths to their steady-state values. To determine how fast this restoration will occur, we first linearize the system, as follows. First we note that x and y can be expressed in terms of the deviations from the steady state in L_1 and L_2 as follows:

$$u = L_1 - L_{ss}$$

$$v = L_2 - L_{ss}$$

$$x = u - v$$

$$y = u + v$$

Assuming the perturbations are small, u and v will be close to zero. The rate of change of the deviations u and v is approximated by the Jacobian:

$$\begin{pmatrix} \dot{u} \\ \dot{v} \end{pmatrix} = \begin{pmatrix} \left.\frac{\partial f}{\partial L_1}\right|_{L_1=L_2=L_{ss}} & \left.\frac{\partial f}{\partial L_2}\right|_{L_1=L_2=L_{ss}} \\ \left.\frac{\partial g}{\partial L_1}\right|_{L_1=L_2=L_{ss}} & \left.\frac{\partial g}{\partial L_2}\right|_{L_1=L_2=L_{ss}} \end{pmatrix} \begin{pmatrix} u \\ v \end{pmatrix}$$

Evaluating the elements around the steady-state value $L_1 = L_2 = L_{ss}$ we obtain the linearized system:

$$\begin{pmatrix} \dot{u} \\ \dot{v} \end{pmatrix} = A \begin{pmatrix} \frac{L_{ss}-P}{L_{ss}^2} & -\frac{1}{L_{ss}} \\ -\frac{1}{L_{ss}} & \frac{L_{ss}-P}{L_{ss}^2} \end{pmatrix} \begin{pmatrix} u \\ v \end{pmatrix}$$

We then express the behavior of x and y in the linear approximation according to

$$\dot{x} = \dot{u} - \dot{v}$$

$$\dot{y} = \dot{u} + \dot{v}$$

This yields, finally, a pair of uncoupled differential equations for x and y:

$$\dot{x} = u\left(\left.\frac{\partial f}{\partial L_1}\right|_{L_1=L_2=L_{ss}} - \left.\frac{\partial g}{\partial L_1}\right|_{L_1=L_2=L_{ss}}\right) + v\left(\left.\frac{\partial f}{\partial L_2}\right|_{L_1=L_2=L_{ss}} - \left.\frac{\partial g}{\partial L_2}\right|_{L_1=L_2=L_{ss}}\right)$$

$$\dot{x} = (u-v)\{A\frac{L_{ss}-P}{L_{ss}^2} + \frac{A}{L_{ss}}\}$$

$$\dot{x} = \{A\frac{L_{ss}-P}{L_{ss}^2} + \frac{A}{L_{ss}}\}x$$

$$\dot{y} = u\left(\left.\frac{\partial f}{\partial L_1}\right|_{L_1=L_2=L_{ss}} + \left.\frac{\partial g}{\partial L_1}\right|_{L_1=L_2=L_{ss}}\right) + v\left(\left.\frac{\partial f}{\partial L_2}\right|_{L_1=L_2=L_{ss}} + \left.\frac{\partial g}{\partial L_2}\right|_{L_1=L_2=L_{ss}}\right)$$

$$\dot{y} = (u-v)\{A\frac{L_{ss}-P}{L_{ss}^2} + \frac{A}{L_{ss}}\}$$

$$\dot{y} = \{A\frac{L_{ss}-P}{L_{ss}^2} - \frac{A}{L_{ss}}\}y$$

we define constants:

$$\alpha = A\frac{L_{SS}-P}{L_{ss}^2} + \frac{A}{L_{ss}}$$

$$\beta = A\frac{L_{SS}-P}{L_{ss}^2} - \frac{A}{L_{ss}}$$

hence:

$$\dot{x} = \alpha x$$

$$\dot{y} = \beta y$$

which by inspection have exponential functions as their solutions:

$$x(t) = x(0)e^{\alpha t}$$

$$y(t) = y(0)e^{\beta t}$$

We now consider what happens if we add random fluctuations to the system. We model intrinsic fluctuations by adding a noise term to the equation governing x, thus:

$$\dot{x} = \alpha x + \sigma \eta$$

where σ denotes the magnitude of the fluctuations and η denotes Gaussian white noise with zero mean and variance of 1. The stationary solution to this equation is well known (Honerkamp, 1994; Van Kampen, 1992) and has a mean of 0 and a mean squared value of:

$$\langle x^2 \rangle = \frac{\sigma^2}{2\alpha}$$

Since we do not know the microscopic molecular source of the fluctuations, we do not know the value of σ, however we assume it is the same for wild type and mutant cells. Hence the mean squared difference in length between the two flagella should be proportional to $\frac{1}{\alpha}$. Substituting the value of α derived above and then using the value of L_{ss} in terms of the

three parameters A, D, and P, we obtain

$$\langle (L_1 - L_2)^2 \rangle \sim \frac{1}{A\frac{L_{ss}-P}{L_{ss}^2} + \frac{A}{L_{ss}}} = \frac{P}{D(2 + \frac{D}{A})}$$

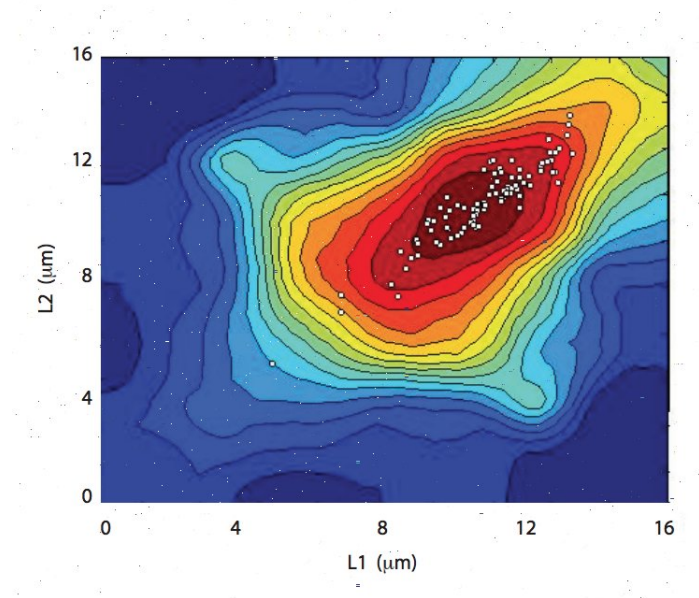Which is given as Equation (2) in the Results section.

Acknowledgments

2.7   Supplemental Information

Figure 2.6: Swimming speed versus flagellar length with lengths of gametes superimposed as white boxes. Swimming speed data is the same as Fig 2.2A, but the gamete datapoints illustrate that the length distribution of gamete flagella is better matched to the regime of optimal swimming.
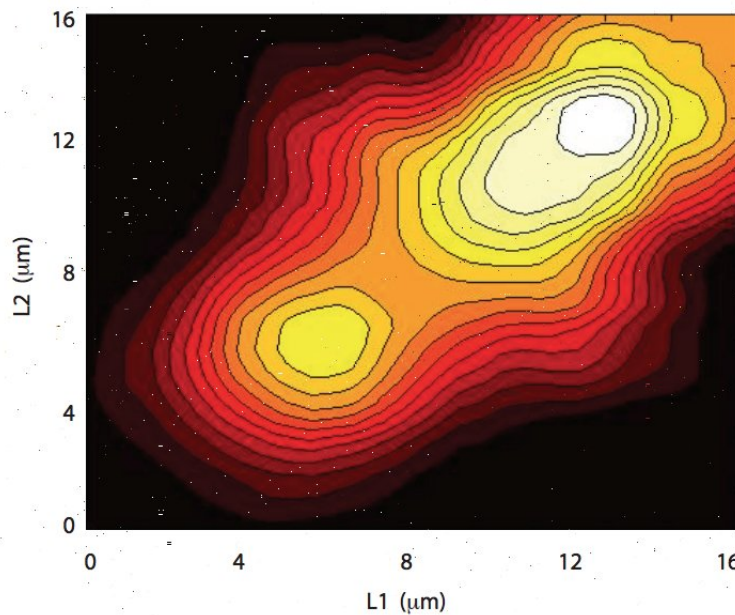
Figure 2.7: Reversal frequency during gliding plotted versus flagellar lengths. White corresponds to maximum frequency of reversal, black minimum. The most reversals occur for cells with flagella of equal lengths, while increased length disparity correlates with decreased reversals.
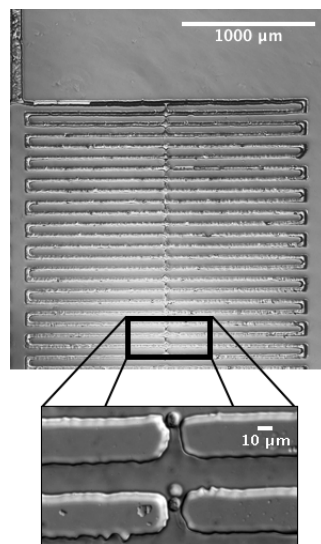
Figure 2.8: (Top) Brightfield image depicting the microfluidic device. Cells and media flow in from the channel at the top left, flow through the serpentine channel with the traps, and exit through a similar channel at the bottom (not shown). (Bottom) Magnified DIC image detailing the trap area with trapped cells.
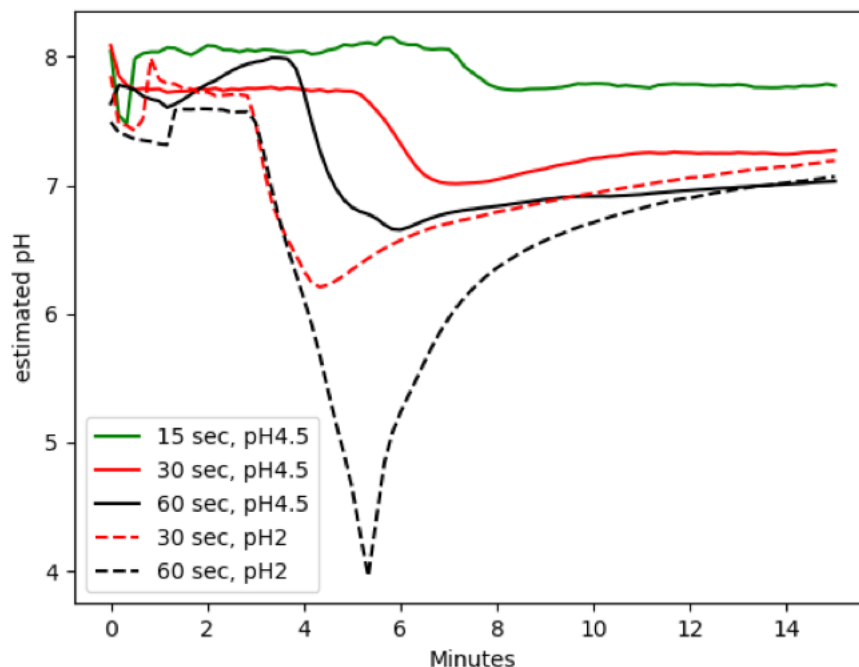
Figure 2.9: Validation of pH shock in the microfluidic device. A stock of fluorescein isothiocyanate (FITC) was prepared and separated into aliquots of increasing pH (3.0-10.5) at 0.5 increments. Each solution was loaded into a syringe and flowed into the device for 10 minutes, after which the fluorescent intensity was measured. The intensity vs pH values were fit to a Henderson-Hasselbalch curve, which yielded a pK_a of 6.45, in agreement with prior reports (Sjoeback 1998). This curve was used to estimate pH values from fluorescent intensities of the same stock of FITC inside the microfluidic device. Two solutions of FITC were prepared from the original stock, one at pH 7.5, one at a lower pH. A pulse of varying time (legend) for each pH tested was delivered to the device, and the pH was measured in 15 second intervals. The time and pH combination that best reproduced the pH shocking protocol for deflagellation was a 60 second pulse of pH 2.0.
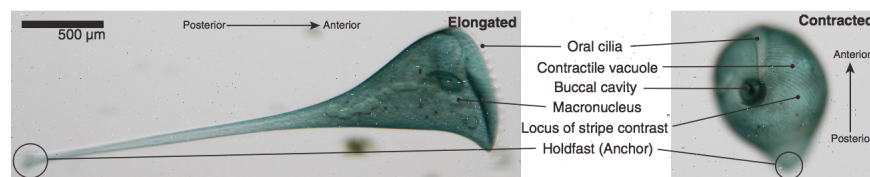
Chapter 3

A Microfluidic Device Enables Long-term Imaging of Stentor

David Bauer, Tatyana Mashukok, Wallace Marshall

3.1 *Stentor* Biology

Stentor coeruleus is an enormous single-celled ciliate, extending up to 1mm in length. . As shown in Fig 3.1, *Stentor* has a holdfast at the posterior end of the cell that it uses to

Figure 3.1: *Stentor* in its elongated state (left), and its contracted state (right). Adapted from Slabodnik *et al.* 2014

attach itself to remain stationary. It eats by beating cilia along the anterior end of the cell to funnel food into its oral apparatus. *Stentor* has a macronucleus with a "beads on a string" morphology.

Notably, if *Stentor* is cut into two pieces, as long as both pieces contain a complete copy of its genome, both pieces will regenerate into two organisms over the course of approximately 8 hours.

Unlike most other organisms that progress through the cell cycle in a few hours, *Stentor* takes four or more days to complete the cell cycle. This presents a major challenge to image *Stentor* throughout their cell cycle, because not only must it be held in place, it must also be fed a constant source of food, as *Stentor* is an obligate predator.

3.2 *Stentor* as a Model Organism

Stentor was widely studied in the early 1900's, but has faded in popularity, probably due to the difficulty in culturing large numbers of *Stentor* and its relatively intractable genetics.

Despite not sharing the ease of culture and wide availability of genetic tools as *S. cerevisiae*, there are many reasons to consider using *Stentor* as a model organism. *Stentor*'s size and ability to regenerate make it an interesting choice for studying some of the key questions underlying fundamental biology, such as how cells regulate their size. *Stentor*'s size allows, in principle, for simple and cheap monitoring. At lower magnification, abberant morphologies are still visible, making high-throughput screens of stentor more economical.

Some have proposed using Stentor as a "canary in a coal mine" type indicator for when

pathogens or harmful impurities are present in water supplies.

Challenges Using *Stentor* as a Model

In addition to the previously mentioned lack of genetic tools and difficulty in culturing,

there are other challenges one must overcome in studying *Stentor*. One way to force *Stentor*

to regenerate is to physically cut the cell into pieces [26]. This introduces a challenge of

reproducibility in performing this technique, as it is difficult to ensure the same contents of

each cut cell, but highlights the extent to which *Stentor* can rebulid itself. One can also

induce regeneration of the oral apparatus via sucrose or urea shock, which is much more

reproducible.

Timelapse imaging of *Stentor* pressents similar challenges to imaging light sensitive cells

— high resolution imaging of *Stentor* morphology can require magnifications with low depth

of field, thus requiring many z-stacks, introducing the problem of phototoxicity. While

phototoxicity is not a problem unique to *Stentor*, it is exacerbated by the fact that *Stentor*

is very camera shy (*Stentor* exhibits negative phototaxis). *Stentor*'s large size necessitates

large doses of light for imaging, such that long time-lapse imaging with z-stacks is probably

not possible on the time-scale of *Stentor* regeneration. Because of its size, it is possible to get

an accurate measure of cell volume at a low magnification with a high depth of field, reducing

the number of z-stacks required. However, if the orientation of *Stentor* is not horizontal, it

is difficult to determine the portion of volume in the z direction.

Complete genetic control over *Stentor* will likely prove difficult due to its genomic redundancy (<100k ploidy), although genomic tools do exist [40].

## 3.3 A Microfluidic Device to Constrain *Stentor* for Imaging

There have not been many instances of people using microfluidics in *Stentor* biology. Blauch *et al.* used microfluidics to study Stentor [27], but their goal was not to keep *Stentor* alive for long-term imaging. There are few such examples in the literature, although there are examples of using microfluidics for long term imaging of other large single-celled organisms, such as *C. elegans* [24][3]. In order address the challenges presented prviously and take advantage of *Stentor*'s unique ability to address the question of cell size control, I constructed a microfluidic device to monitor the regeneration of *Stentor* after microsurgery and sucrose shock. Fig 3.2 contains an example of the repeating element of the device. A single device can contain up to 20 *Stentor* in individual chambers. Each chamber is approximately 750μm x 750μm in area, with a height of 125μm. Each chamber is connected in parallel to a main media flow channel. The dimensions of the chamber were selected to house one approximately fully-extended *Stentor*. The dimensions of the main channels were selected such that the ratios of the hydrodynamic resistances of the chamber channels to the main channel would

yield approximately the same flow rate through each chamber channel as described in [14]. There are barriers to prevent *Stentor* from escaping the chamber, which are separated by approximately 15μm. *Stentor* must be individually loaded into each chamber via a loading channel, shown in Fig 3.2, inset. *Stentor* can be loaded via a pipette. This flow path must be sealed to prevent media flow from the main channel through the loading channel, which would flush the *Stentor* out of the device. While microfluidic valves [29][28] would be ideal for this scenario, we opted for a physical plug (melted 2μL pippette tip, see 3.6) for flexibility.

3.4   Results

In this section I will discuss the preliminary testing results of this chamber. In simple experiments assessing the viability of the device, after filling the device with media, we loaded *Stentor* into the device under no flow. We then observed the cells in brightfield microscopy until air bubbles from evaporation displaced most of the *Stentor*, which took approximately 72 hours. Before the *Stentor* were displaced, they did not display any signs of distress, such as shedding their oral apparatus or swimming backwards. To test both the viability and effectiveness of solution exchange of the device, we decided to test *mob1* RNAi by feeding, as described in [40]. This was selected because the *mob1* RNAi knockout has a strong morphological phenotype, allowing a by-eye determination of success. We then filled a 60mL syringe with the bacteria and used a syringe pump to flow the solution through the
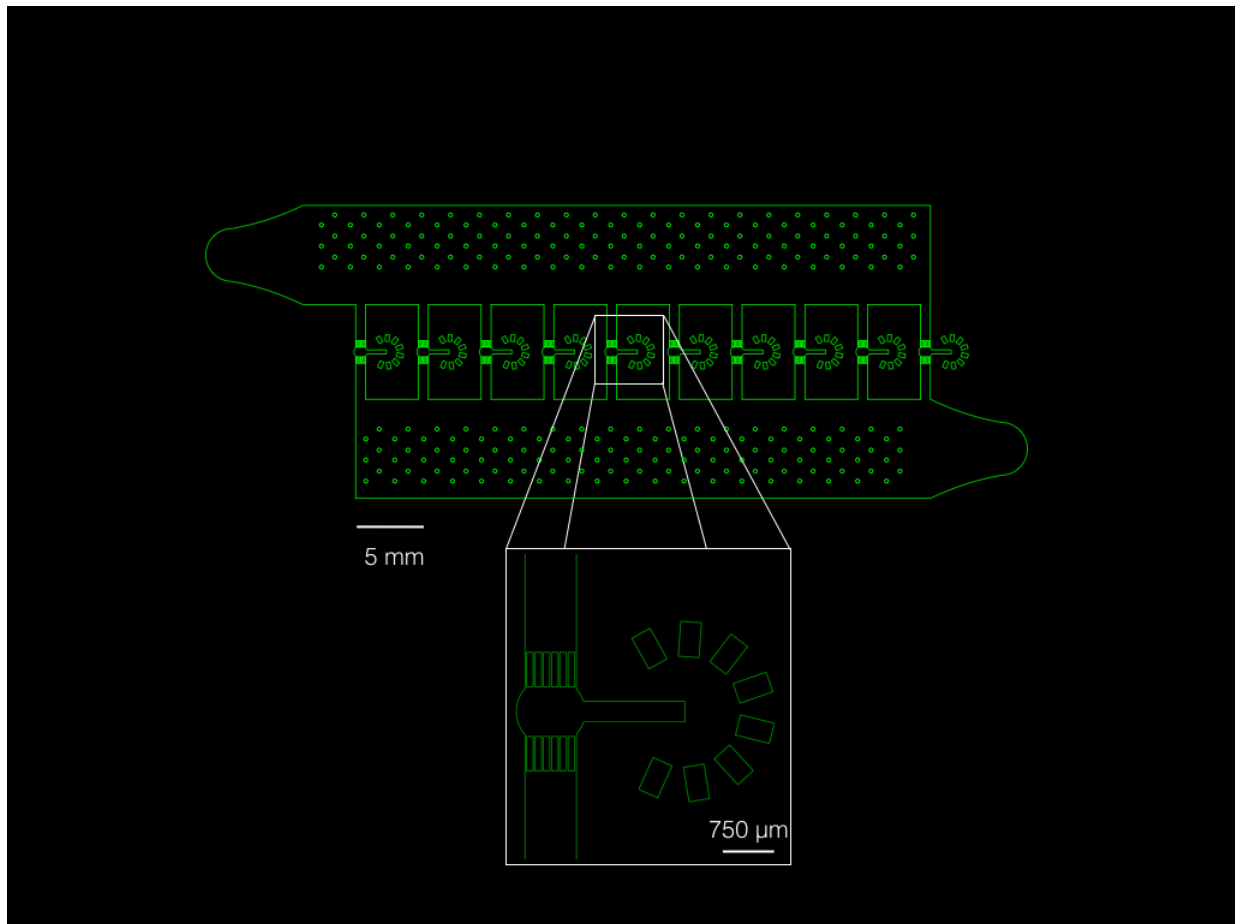
Figure 3.2: A CAD drawing of the version of the device used in the experiments described in this dissertation. The main media flow is from top left to bottom right. (inset) The loading channel and main chamber are shown in greater detail. A hole is punched at the center of the punch guide (circumferential rectangles), and a *Stentor* is loaded through the channel. This hole must be sealed to prevent the *Stentor* from escaping.
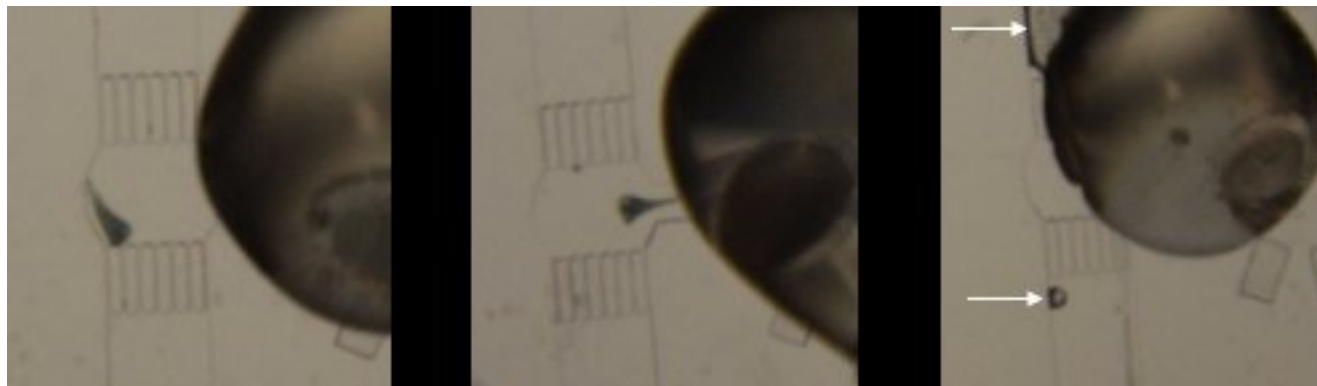
Figure 3.3: An example of *Stentor* trapped in the device. (left) and (middle) *Stentor* are trapped in the main chamber. (right) arrows indicate air bubbles. (all) large areas on the right-hand side are hot-glue drops, which were used to seal the *Stentor* loading hole for this experiment. See section 3.6 for a discussion on sealing methods.

Stentor chambers at a bulk rate of $100\frac{\mu L}{hr}$. The *Stentor* were left to grow under constant flow of this media for 48 hours. After 48 hours of feeding, none of the ten *Stentor* unambiguously displayed the phenotype. This is fewer than expected based on previous reports [40], where at least 90% displayed the phentotype after 48 hours. Based on these results, we have redesigned the trap, shown in Fig 3.4. In order to discourage Stentor from moving back into the loading channel, we tapered the end of the channel to 50μm. This is not enough of a restriction to injure *Stentor*, but based on initial observations, it is both small enough and long enough to keep *Stentor* from exploring the loading channel.

3.5 Discussion

We believe these experiments showed that this microfluidic device constrains *Stentor* in both xy and z for more than 48 hours for timelapse imaging while providing fresh media. This
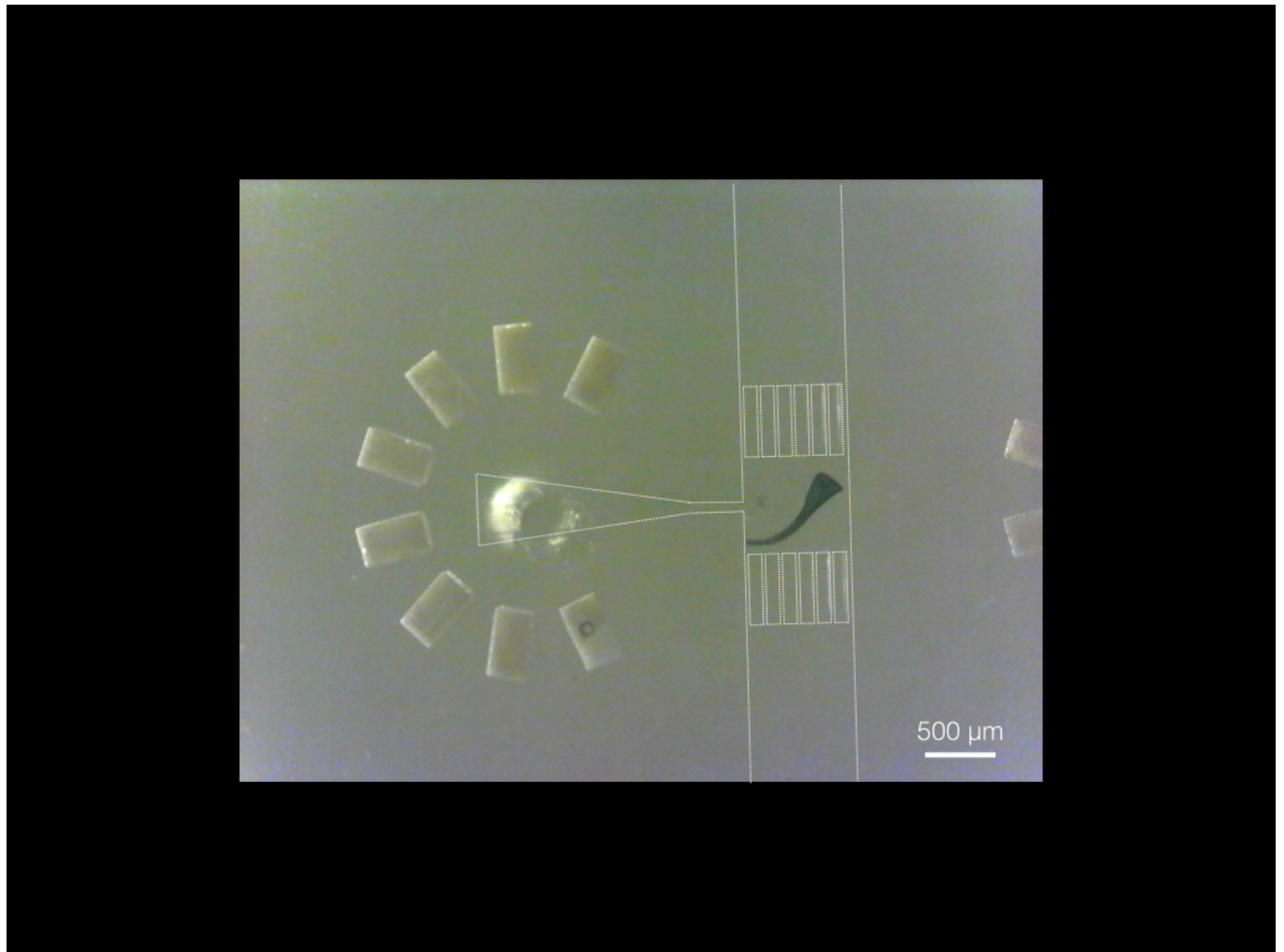
Figure 3.4: A single *Stentor* in the new device. Due to low contrast imaging, the features
of the trap are difficult to see have thus been emphasized by white dotted lines.

greatly simplifies many experiments by providing a robust way to localize the cell for imaging

in xy and z, eliminating the need for cell tracking. While there are existing methods to confine

Stentor [1] in z, they typically do not include xy. In addition, it is difficult to achieve the

repeatability of z-height from photo-lithography molds. These methods that geometrically

restrict *Stentor* without flow are subjecting *Stentor* to increasingly anoxic environments,

which can lead to cell death during long time series experiments [2][35]. Additionally, we

believe that our device will allow for more precise monitoring of the perturbations that small

molecules have on *Stentor*.

In our first RNAi feeding experiment, we had a lower fraction of cells showing a phenotype

than prior reports [40]. Although a lack of observed phenotype is sometimes observed in

RNAi feeding outside of the microfluidic device, for the purpose of improving the microfluidic

device I will discuss factors that could have contributed to the lack of observed phenotype.

The flow of the media containing the bacteria was likely too high for *Stentor* to create a local

flow of bacteria towards its mouth. Furthermore, we noticed that flow across all channels

was not equal, so it is possible that some *Stentor* did not get enough bacteria. I most likely

incorrectly calculated the hydrodynamic resistance of the barriers and thus the channels,

which causes the flow to be unevenly distributed among the channels. We can confirm this

hypothesis by measuring fluorescent bead traces to infer the flow through each channel. In

long time series experiments of greater than 12 hours, we found that air bubbles began to

form from evaporation, and that this could interrupt flow paths or displace *Stentor* from the

imaging chamber. We were able to prevent evaporation by lasercutting an acrylic "parapet"

(see Section 3.6) to keep a pool of water on top of the PDMS device. This has the effect of degrading transmitted-light microscopy, but fluorescent imaging is unaffected.

3.6 Materials and Methods

Fabrication and Design of Microfluidic Device

For Design: The device was modeled in Auto-CAD and printed on a plastic transparency film. For Mold: The device was fabricated using standard photo-lithographic methods for a single-layer device. Spin coat a layer of SU8 3050 @ 1000rpm. Measured feature height of 15μm. Soft bake at 95°C for 30min, and expose $250\frac{mJ}{cm^2}$. Post-exposure bake at 95°C for 5 minutes. Develop until no precipitate is visible upon isopropanol rinse. Finally, hard bake for 3 hours. For PDMS device: Mix 10:1 monomer to crosslinker of Silgard 184. Degas in a vacuum chamber for 1 hr. Bake at 85°C for 1.5 hrs. Cut away excess PDMS and punch holes for tubing. For plasma bonding: (look up other method) Place in plasma cleaner, pull vacuum. After pressure falls below 0.1 mbar, flow O_2 into chamber at 1 mbar. Turn on RF field for 45 seconds.

Operation of Microfluidic Device

Flow was driven by a New Era OEM syringe pump (NE-500) at a speed of $1000\frac{\mu m}{hr}$. The pump drives a 60ml syringe with a 27G needle, which is connected to the device via polyethylene

tubing (Scientific Commodities BB31695-PE/2). The *Stentor* loading hole was plugged with partially melted 2μL pipette tips. Tips were held over a Bunsen burner for 1-3 seconds, then tested for a watertight seal. This method is the most reliable compared to hot glue (not reliably watertight, obstructs transmitted light) and epoxy (highly toxic to *Stentor*). To prevent air bubbles: We laser cut four pieces of acrylic, one for each side of a rectangular, watertight "housing" around the PDMS. The acrylic was glued to itself with a solvent-based glue, and to the glass with regular adhesive (hot glue).

RNAi by Feeding

RNAi was performed by transforming HT115 E. coli with each plasmid to allow for dsRNA expression of the target gene. Transformed bacteria were grown to log phase and then induced with 1 mM IPTG for 3 h at 37 °C. After induction, bacteria were washed and resuspended in media, then fed to *Stentor* that had been previously starved for 24–48 h.

Culture of Stentor

Stentor and media (purified spring water) were both purchased from Carolina Biological Supply. *Stentor* were cultured in 500mL of purified spring water, splitting every other week to a density of approximately 100 cells in fresh media. *Stentor* were fed 10^8 *Chlamydomonas* cells once per week.

Bibliography

[1] "A New Rotary Microcompressor". In: *Transactions of the American Microscopical Society* 97.3 (1978), pp. 412–416.

[2] "A Portable Apparatus for the Determination of Oxygen Dissolved in a Small Volume of Water". In: *Journal of Experimental Biology* 15 (1938), pp. 437–445.

[3] "Automated On-Chip Rapid Microscopy, Phenotyping and Sorting of C. Elegans". In: *Nature Methods* 5.7 (2008), pp. 637–643.

[4] "Avalanche-like behavior in ciliary import". In: *PNAS* 110.10 (2013), pp. 3925–3930.

[5] L. Baala et al. "Pleiotropic effects of CEP290 (NPHP6) mutations extend to Meckel syndrome". In: *American Journal of Human Genetics* 81 (2007), pp. 170–179.

[6] "Cell growth and division: III. Conditions for balanced exponential growth in a mathematical model". In: *Biophysical Journal* 8 (1968), pp. 431–444.

[7] Chin-Wen Chang et al. "Automatic segmentation of abnormal cell nuclei from microscopic image analysis for cervical cancer screening". In: *2009 IEEE 3rd International Conference on Nano/Molecular Medicine and Engineering*. 2009, pp. 77–80.

[8] "Chlamydomonas as a model organism". In: *Annual Review of Plant Physiology and Plant Molecular Biology* 52 (2001), pp. 363–406.

[9] "Control of Organelle Size: The Golgi Complex". In: *Annual Review of Cell and Developmental Biology* 27 (2011), pp. 57–77.

[10] "Controlling cell size through sizer mechanisms". In: *Current Opinion in Systems Biology* 5 (2017), pp. 86–92.

[11] B Craige and G. Witman. "CEP290 tethers flagellar transition zone microtubules to the membrane and regulates flagellar protein content". In: *Journal of Cell Biology* 190 (2010), pp. 927–940.

[12] "Crescerin uses a TOG domain array to regulate microtubules in the primary cilium". In: *Molecular Biology of the Cell* 26 (2015), pp. 4248–4264.

[13] "Flagellar Elongation as a Moving Boundary Problem". In: *Bulletin of Mathematical Biology* 36 (1974), pp. 265–273.

[14] "Flow distribution in parallel microfluidic networks and its affects on concentration gradient". In: *Biomicrolfuidics* 9 (2015), p. 054119.

[15] Juliana Helou et al. "Mutation analysis of NPHP6/CEP290 in patients with Joubert syndrome and Senior–Løken syndrome". In: *Journal of Medical Genetics* 44.10 (2007), pp. 657–663.

[16]   N. L. Hendel, M. Thomson, and W. F. Marshall. "Diffusion as a Ruler: Modeling Kinesin Diffusion as a Length Sensor for Intraflagellar Transport." In: *Biophysical Journal* 114.3 (2018), pp. 663–674.

[17]   A.I. den Hollander et al. "Mutations in the CEP290 (NPHP6) gene are a frequent cause of Leber congenital amaurosis". In: *American Journal of Human Genetics* 79 (2006), pp. 556–561.

[18]   "Identification of Signaling Pathways Regulating Primary Cilium Length and Flow-Mediated Adaptation". In: *Current Biology* 20 (2010), pp. 182–187.

[19]   H. Ishikawa and W. F. Marshall. "Ciliogenesis: building the cell's antenna". In: *Nature Reviews Molecular Cell Biology* 12.4 (2011), pp. 222–234.

[20]   H. Ishikawa and W. F. Marshall. "Testing the time-of-flight model for flagellar length sensing". In: *Molecular Biology of the Cell* 28 (2017), pp. 3447–3456.

[21]   "Learning from Noise: How Observing Stochasticity May Aid Microbiology". In: *Trends in Microbiology* 26.4 (2018), pp. 376–385.

[22]   "Length Determination in Bacteriophage Lambda Tails". In: *Cell* 39.2 (1984), pp. 691–698.

[23]   "Length regulation of multiple flagella that self-assemble from a shared pool of components". In: *e-Life* 8 (2019), e42599.

[24]   "Lifespan-on-a-chip: microfluidic chambers for performing lifelong observation of C. elegans". In: *Lab Chip* 10 (2010), pp. 589–597.

[25]   W. B. Ludington et al. "A Systematic Comparison of Mathematical Models for Inherent Measurement of Ciliary Length: How a Cell Can Measure Length and Volume". In: *Biophysical Journal* 108.6 (2015), pp. 1361–1379.

[26]   "Methods for the Study of Regeneration in Stentor". In: *Journal of Visualized Experiments* 136 (2018), p. 57759.

[27]   "Microfluidic guillotine for single-cell wound repair studies". In: *PNAS* 114 (2017), pp. 7283–7288.

[28]   "Microfluidic Large-Scale Integration". In: *Science* 298 (2002), pp. 580–584.

[29]   "Microvalves and Micropumps for BioMEMS". In: *Micromachines* 2 (2011), pp. 179–220.

[30]   "Mitochondrial network morphology: building an integrative, geometrical view". In: *BMC Biology* 11.71 (2013).

[31]   "Negative regulation of ciliary length by ciliary male germ cell-associated kinase (Mak) is required for retinal photoreceptor survival". In: *PNAS* 107 (2010), pp. 22671–22676.

[32]   "Organelle Growth Control through Limiting Pools of Cytoplasmic Components". In: *Current Biology* 22.9 (2012), R330–R339.

[33] S. et al Perlmutter. "Measurements of Ω and Λ from 42 High-Redshift Supernovae". In: *Astrophysical Journal* (1999), pp. 565–586.

[34] "Relations between axon length and axon caliber". In: *Journal of the Neurological Sciences* 63 (1984), pp. 369–380.

[35] "Respiratory Energy Losses in Stentor coeruleus". In: *Oecologia* 21.3 (1975), pp. 273–278.

[36] "Robust organelle size control via bursty growth". In: *bioRxiv* (2019).

[37] J. Rosenbaum, J. Moulder, and D. Ringo. "Flagellar Elongation And Shortening In Chlamydomonas: The Use of Cycloheximide and Colchicine to Study the Synthesis and Assembly of Flagellar Proteins". In: *The Journal Of Cell Biology* 41 (1969).

[38] "Stochastic Gene Expression in a Single Cell". In: *Science* 297 (2002), pp. 1183–1186.

[39] "The Dependence of Type Ia Supernova Luminosities on their Host Galaxies". In: *Monthly Notices of the Royal Astronomical Society* 1.23 (2011).

[40] "The Kinase Regulator Mob1 Acts as a Patterning Protein for Stentor Morphogenesis". In: *PLOS Biology* 12.5 (2014), e1001861.

[41] "The Limiting-Pool Mechanism Fails to Control the Size of Multiple Organelles". In: *Cell Systems* 4 (2017), pp. 559–567.

[42] *Ueber neue Probleme des Zellenlehre*. Vol. 1. Arch Zellforsch, 1908, pp. 1–32.

Publishing Agreement

It is the policy of the University to encourage open access and broad distribution of all theses, dissertations, and manuscripts. The Graduate Division will facilitate the distribution of UCSF theses, dissertations, and manuscripts to the UCSF Library for open access and distribution. UCSF will make such theses, dissertations, and manuscripts accessible to the public and will take reasonable steps to preserve these works in perpetuity.

I hereby grant the non-exclusive, perpetual right to The Regents of the University of California to reproduce, publicly display, distribute, preserve, and publish copies of my thesis, dissertation, or manuscript in any form or media, now existing or later derived, including access online for teaching, research, and public service purposes.

DocuSigned by:

David Bauer

4A56C2CB9C88425...

Author Signature

6/9/2020

Date